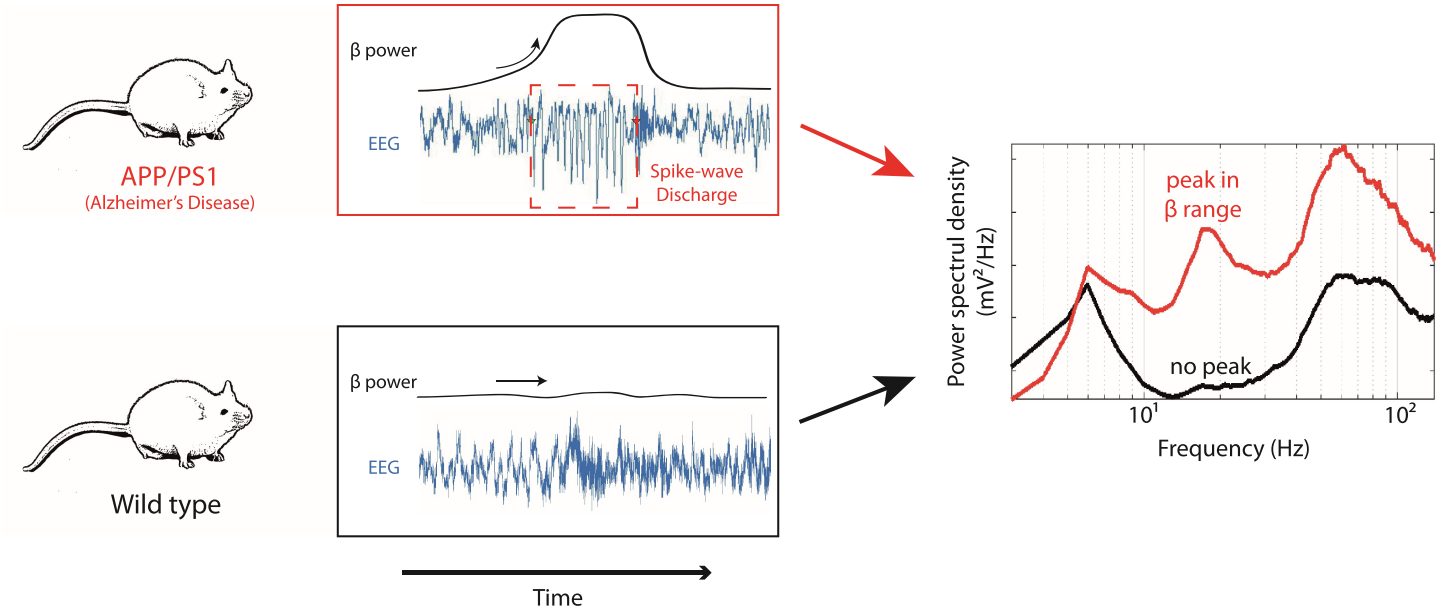
APP/PS1
(Alzheimer's Disease)
β power
EEG
Spike-wave
Discharge
Wild type
β power
EEG
Time
Power spectrul density
(mV²/Hz)
peak in
β range
no peak
10¹
10²
Frequency (Hz)

Highlights

- Cortical 8 – 60 Hz oscillations are augmented in APP/PS1 mice independent of age
- APP/PS1 mice but not wild-type mice display frequent spike-wave discharges
- Increased theta and beta oscillations precede spike-wave discharges
- Auditory EPs of APP/PS1 mice stay augmented but acoustic startles diminish with age

Increased cortical beta power and spike-wave discharges in middle-aged APP/PS1 mice

Nanxiang Jin[1]*, Arto Lipponen[1,2]*, Hennariikka Koivisto[1], Kestutis Gurevicius[1], Heikki Tanila[1]

[1]A. I. Virtanen Institute, University of Eastern Finland, Kuopio, Finland
[2] present address: Department of Psychology, University of Jyväskylä, Finland

* equal contribution

Correspondence:

Heikki Tanila, MD, PhD
Professor of Translational Neuroscience
A. I. Virtanen Institute
University of Eastern Finland
Neulaniementie 2, 70210 Kuopio
FINLAND
email: Heikki.Tanila@uef.fi
tel: +358-40-3552084

Running title: Spike-wave discharges in aged APP/PS1 mice

Abstract

Amyloid plaque forming transgenic mice display neuronal hyperexcitability, epilepsy and sudden deaths in early adulthood. However, it is unknown whether hyperexcitability persists until middle ages when memory impairment manifests. We recorded multichannel video-EEG, local field potentials and auditory evoked potentials in transgenic mice carrying mutated human APP and PS1 genes and wild-type littermates at 14-16 months and compared the results with data we have earlier collected from 4-month-old mice. Further, we monitored acoustic startle responses in other APP/PS1 and wild-type mice from 3 to 11 months of age. Independent of the age APP/PS1 mice demonstrated increased cortical power at 8–60 Hz. They also displayed over 5-fold increase in the occurrence of spike-wave discharges and augmented auditory evoked potentials compared to nontransgenic littermates. In contrast to evoked potentials, APP/PS1 mice showed normalization of acoustic startle responses with aging. Increased cortical power and spike-wave discharges provide powerful new biomarkers to monitor progression of amyloid pathology in preclinical intervention studies.

Key words: Alzheimer's disease, amyloid plaque, transgenic, epilepsy, EEG

Abbreviations

AEP = auditory evoked potential

APP = amyloid precursor protein

dVC = deep visual cortex

LFP = local field potential

mFC = medial frontal cortex

PSD = power spectral density

PS1 = presenilin-1

sFC = superficial frontal cortex

sVC = superficial visual cortex

SWD = spike-wave discharge

1. Introduction

Alzheimer's disease is often considered a slow degeneration process where the activity of neurons gradually fades away. However, accumulating evidence suggests that the early stages of the disease are actually characterized by neuronal hyperactivity. Functional magnetic resonance imaging (fMRI) studies in humans have revealed increased activation of medial temporal lobe structures in patients with mild cognitive impairment compared to elderly controls or patients with diagnosed Alzheimer's disease (Dickerson et al., 2005; Hämäläinen et al., 2007). In extreme cases, the neuronal hyperactivity (or hyperexcitability) may manifest as epileptic seizures. Overall, epileptic seizures in Alzheimer patients are rare but still ~8 times more common than in general age-matched population (Scarmeas et al., 2009). However, the occurrence of seizures and myoclonus is particularly high in early-onset, autosomal dominant familial AD linked with amyloid precursor protein (*APP*) or presenilin-1 (*PS1*) mutations, with estimated seizure rates ranging between 15–67 % and myoclonus rates between 9–31%, being highest in *PS1* mutation carriers (Vossel et al., 2017). Moreover, a recent prospective EEG study found subclinical epileptiform activity in more than 40% of AD patients (Vossel et al., 2016).

Increased epileptic activity, including spontaneous seizures, have been documented in most transgenic mice carrying mutated human amyloid precursor protein (APP) gene (Ittner et al., 2014; Minkeviciene et al., 2009; Nygaard et al., 2015; Palop et al., 2007; Westmark et al., 2010; Ziyatdinova et al., 2016). Further, these mice show decreased threshold for seizure induction (Palop et al., 2007; Westmark et al., 2008; Ziyatdinova et al., 2016), and in vivo imaging of cortical neurons in APP transgenic mice show spontaneous hyperactivity of neurons around amyloid plaques (Busche et al., 2008). Indices of neuronal hyperexcitability can be also seen in *in vivo* EEG recordings in freely moving APP transgenic mice. Most commonly reported findings are brain region and state dependent changes in theta power (Gurevicius et al., 2013; Hazra et al., 2016; Jyoti et al., 2010; Papazoglou et al., 2017, 2016; Wang et al., 2002), and consistent state-independent increase in beta-power (Corbett et al., 2013; Gurevicius et al., 2013; Jyoti et al., 2010; Wang et al., 2002) up to gamma-range, if recorded (Corbett et al., 2013; Gurevicius et al., 2013; Papazoglou et al., 2016). Moreover, these mice display increased cortical spiking (Born et al., 2014; Sanchez et al., 2012), and increased amplitude of auditory (Gurevicius et al., 2013; Wang et al., 2002) and somatosensory (Maatuf et al., 2016) evoked potentials, which speak for increased cortical excitability.

Notably, almost all EEG studies in AD model mice have been conducted in young adult animals with moderate amyloid accumulation, and we do not know whether hyperexcitability continues until ages above 12 months when both amyloid pathology and memory impairment have fully developed. From the translational viewpoint it is important to make the distinction between phenotypes that manifest mainly in young animals (suggesting developmental or transgene effect independent of amyloid pathology) and phenotypes that show progression with age and amyloid pathology.

We have earlier reported increased cortical and thalamic power between 6-70 Hz and augmented auditory evoked potentials (Gurevicius et al., 2013) in 4-month-old $APP_{Swe}/PS1_{dE9}$ mice with well-characterized epilepsy phenotype (Minkeviciene et al., 2009). To assess changes in cortical, thalamic and hippocampal excitability in this mouse with aging we replicated the power spectral and evoked potential analysis at the age of 14-16 months, when the amyloid pathology has fully developed, and the mice, in contrast to 4-month-old ones, show robust memory impairment (Minkeviciene et al., 2008). As a behavioral measure of brain excitability and to assess myoclonus associated with some forms of familial AD (Vossel et al., 2017), we also followed-up acoustic and spontaneous startles in a separate group of $APP_{Swe}/PS1_{dE9}$ mice from 3 to 11 months of age. Here we provide evidence for continued cortical hyperexcitability in APP/PS1 mice up to 16 months of age compared to 4-month-old transgenic mice or middle-aged wild-type littermates. A novel finding was frequent cortical spike-wave discharges in APP/PS1 mice at both ages and their co-occurrence with increased oscillations at 6-12 Hz and 20-40 Hz.

2. Methods

2.1 Animals

The subjects were $APP_{Swe}/PS1_{dE9}$ (APP/PS1) mice (Jankowsky et al., 2004) and their age-matched wild-type littermates. The APP/PS1 colony was based on founders obtained from D. Borchelt and J. Jankowsky (Johns Hopkins University, Baltimore, MD, USA). The mice were backcrossed to C57BL/6J strain for 16 generations. The main EEG/LFP study comprised 14 male APP/PS1 mice and 16 wild-type littermate controls between 14 and 16 months of age, while the experiment on acoustic startle reflexes included 9 female APP/PS1 mice and 8 wild-type littermates. In addition, we reanalyzed select data from 10 APP/PS1 and 7 WT female mice who were recorded at 4 months of age in our previous study (Gurevicius et al., 2013). The mice were kept in a controlled

environment (constant temperature, 22 ± 1 °C, humidity 50 – 60 %, lights on 07:00-19:00), with food and water available ad libitum. All animal procedures were carried out in accordance with the guidelines of the European Community Council Directives 86/609/EEC and approved by the Animal Experiment Board of Finland.

To obtain quantitative data on the occurrence of sudden deaths in our breeding colony of APP/PS1 mice, we took advance of an electronic animal data management system (Provet, Espoo, Finland) that has been in use since mid-2010. We screened all APP/PS1 transgenic (genotype confirmed with PCR) that were not sacrificed for sampling before the age of 12 months for recorded spontaneous deaths or euthanasia due to impaired health condition after an eyewitness report of convulsions. Mice with an operation requiring general anesthesia within three weeks from the reported sudden death were excluded from the analysis.

2.2 Electrode implantation

Surgery was performed under isoflurane anesthesia (4.5% for induction, ~2% for maintenance). Animals were chronically implanted with a double or triple wire electrodes (Formwar® insulated stainless steel wire, diameter 50 µm, California Fine Wire Company Co, Grover Beach, CA, USA) at the following locations: medial frontal cortex, two doublet electrodes in parallel with a vertical tip separation of 400 µm at AP +1.8 from bregma, ML + (right) 0.8 from midline and +0.2, and DV 1.9 (deeper tip) from dura; hippocampus, a triplet electrode with a vertical tip separation of 400 µm at AP -1.8, ML +1.0, and DV 2.2 (the deepest tip); lateral geniculate nucleus of thalamus, a doublet electrode with a vertical tip separation of 400 µm at AP -2.3, ML – (left) 2.3, and DV 2.8 (deeper tip); visual cortex, a triplet electrode with a vertical tip separation of 200 µm at AP -3.8, ML -2.3, and DV 0.6 (the deepest tip). In addition, cortical screw electrodes were attached to the left frontal bone (AP +1.0, ML -2.0) and right parietal bone (AP -1.0, ML +2.5). Further, two screws were fixed on the occipital bone to serve as the ground and common reference. The screws served also as the anchors for dental acrylic cement and the connector (Mill-Max, NY, USA). In addition, stainless steel wire (Formwar® insulated, diameter 50 µm, California Fine Wire Company Co, Grover Beach, CA, USA) was inserted during surgery between the neck muscles of for electromyogram (EMG) recording. After the surgery, the mouse received carprofen daily (5 mg/kg, i.p., Rimadyl®, Vericore, Dundee, UK) for postoperative analgesia max 3 days and antibiotic powder (bacitrasin 250 IU/ g and neomycinsulfate 5mg/g, Bacibact®, Orion Finland) was applied on the wound.

2.3 Video-EEG and AEP acquisition

After a recovery period of 7 days the animals were accustomed to the recording setup. The animal was freely moving in a round metal arena (diameter = 18.5 cm), connected to a lightweight recording cable with a counter-weight pulley system. The implanted connector (Mill-Max, NY, USA) was attached to a preamplifier (Plexon HST/16o50-G1-R11, Dallas, USA,) and the signal was further amplified with an AC amplifier (A-M Systems 3600, Sequim, WA, USA; gain 1000, band-pass 1 – 3000 Hz). At least three sessions of undisturbed 1.5 h daytime (light phase) recording was collected and digitized at 2 kHz per channel (DT2821series A/D board; Data Translation, Marlboro, MA, USA). The data were acquired by using Sciworks 5.0 program (DataWave Technologies, Loveland, CO, USA). The behavior of the animals was recorded using a camera (Live!Cam, Video IM Pro, Creative, Dublin, Ireland) that was positioned on top of the arena and synchronized with electrophysiological signals. Auditory evoked potentials (AEPs) were evoked using a pair of click tones (3 kHz, duration 10 ms, 70 dB, 500 ms between the pairs, interstimulus interval 10 s). For AEP recordings the mouse was continuously observed and all records for further analysis were obtained during immobility of the animal. A total of 30 responses at the parietal screw electrode were sampled and averaged.

2.4 Histology

At the end of the experiment the animals were deeply anesthetized with Equithesin solution (0.1 ml / 10g) (chloral hydrate 425 mg + phenobarbital 60 mg/ml 1.75 ml + propylene glycol 3.3 ml + ethanol 100 % 1.2 ml, filled till 10 ml volume with distilled water). The locations of electrodes were marked by passing 50 µA DC current 8-10 s through all channels with wire electrodes. The mouse was perfused with ice-cold saline for 5 min at 10 ml/min followed by 4 % paraformaldehyde (PFA) solution for 9 min at 10 ml/min. The brain was removed and left for immersion postfixation for 4 h in 4 % PFA and after that in 30 % sucrose solution for 24 h. The brains were stored in a cryoprotectant at -20 °C until slicing. Coronal sections (thickness 35 µm) were cut with a freezing slide microtome.

Every third hippocampal section was stained for GFAP (glial fibrillary acidic protein) to reveal the gliosis around chronic wire electrodes. Mouse anti-GFAP was bought from Sigma-Aldrich (1:1000, MO, USA) and goat anti-mouse with horseradish peroxidase from Pierce Biotechnology (1:500, Rockford, IL, USA). In addition, select sections were stained for the N-terminal human Aβ specific antibody W02 (Genetics, Switzerland) to visualize amyloid plaques. The sections were examined using an Olympus microscope at 25-40 x magnification. In addition to lesion marks and gliosis in

histology, we used well-known hippocampal electrophysiological markers to verify electrode location. Polarity and amplitude of theta oscillation and presence of ripple oscillations defined hippocampal layers, while reversal of the visual evoked potential (Leinonen et al., 2016) was used to distinguish superficial (sVC) and deep (dVC) layers of the visual cortex.

All signals were normalized to amplification and analyzed offline in Matlab (Mathworks, Natick, MA, USA; R2015b). In the beginning, all LFP/EEG recordings during spontaneous behaviors were processed to artifact/noise estimation. Every channel in each recording was divided into 10-s sweeps to facilitate artifact exclusion, behavioral state assignment and further analysis. To eliminate occasional artifacts (e.g. bad contact, jerky movements, animal handling, etc.), we calculated the averaged power spectrum distribution between 80 and 90 Hz for each sweep, and outlying sweeps were excluded with iterative implementation of the Grubbs test for outliers (MATLAB routine "deleteoutliers.m" by Brett Shoelson); besides, we visually checked recording quality and cut out noisy sweeps manually from individual channels. All channels that had fewer than 60 noisy sweeps (=10 min) were qualified into the database; however, only the first recording session that fulfilled the criteria was processed for further analysis.

Next, we assigned each sweep to one of the four behavioral states: movement, waking immobility, rapid eye movement (REM) sleep, or non-REM (NREM) sleep, based on a semi-automated procedure as following: (1) the sweeps with EMG (1–100 Hz) amplitude above the mean were assigned as movement; (2) an alpha (10–15 Hz)/ gamma (30–100 Hz) power ratio above the mean characterized NREM sleep. If the ratio between two NREM sweeps remained 25% above the smallest value, those sweeps were merged together; (3) a high-theta (7–9 Hz)/delta (1–4 Hz) power ratio above the mean by 2 SDs characterized REM sleep, and two REM sweeps were merged together if the ratio remained above the mean in between. In addition, the preceding sweep had to be classified as NREM sleep; otherwise, sweeps with high theta/delta ratios were assigned as waking immobility; (4) all remaining waking time was assigned as waking immobility. The behavioral assignment was further verified by visual inspection on the resulting hypnogram, raw LFP/EEG data, and video and was corrected if needed as done in our previous study (Gurevicius et al., 2013). The power spectral density (PSD) was calculated on each sweep with Welch's averaged modified periodogram method of spectral estimation (default MATLAB parameters), and then averaged within each behavioral state, brain region and genotype. To compare the PSD between the genotypes, we ran multiple t-tests for each 1 Hz bin and applied false discovery rate correction (Benjamini and Hochberg, 1995) for multiple comparisons. The statistical threshold was set at $p < 0.05$. To enable comparison across ages and across two studies done in the same laboratory but with

a different amplifier (with possibly different calibration) we normalized the PSDs of the 4-month-old mice so that the group means of WT mice of the two ages became equal. This approached may have masked any age-related systematic effect. However, based on our earlier longitudinal study from 6 to 13 months of age, there is no major age-related change in the cortical EEG power, as long as the animals are in the same behavioral state (Wang et al., 2002). We divided the PSD into conventional frequency bands, delta (1-4 Hz), theta (5-9 Hz), alpha (10-15 Hz), beta (16 – 29 Hz), and gamma (30 – 100 Hz) and compared the power in these bands between the old dataset on young mice and the present one on middle-aged mice. The data were analyzed by two-way ANOVA, with genotype and age as factors.

Cortical spike-wave discharge (SWD) with a characteristic dominant frequency of 3-4 Hz is the electrophysiological characteristics of absence epilepsy in humans (Timofeev and Steriade, 2004). In many aspects identical SWD complex with alternating spikes and waves can be seen in genetic rodent models of absence epilepsy but with different frequency characteristics. The basic frequency of the wave component starts around 10-12 Hz and quickly stabilizes to 7 – 8 Hz. A second harmonic peak can often be seen around 20 Hz (Lüttjohann et al., 2013). We screened out the SWD events from the cortical EEG with the help of these two frequency bands as follows. First, raw EEG data were bandpass filtered between 7 – 23 Hz, and then an envelope was calculated by taking absolute values of Hilbert-transformed filtered data. Second, a positive threshold was set above the envelope mean. The two crossing points between the envelope and the threshold marked the range of a candidate SWD event. If the time gap between consecutive candidate events (end of the first to the beginning of the second) was smaller than 500 ms, these candidate events were merged. Besides, events that were shorter than 400 ms or have fewer than three spike-wave cycles were excluded from the SWD collection. First, raw EEG data were bandpass filtered between 7 – 23 Hz, and then an envelope was calculated by taking absolute values of Hilbert-transformed filtered data. Second, a positive threshold was set above the envelope mean. The two crossing points between the envelope and the threshold marked the range of a candidate SWD event. If the time gap between consecutive candidate events (end of the first to the beginning of the second) was smaller than 400 ms, these candidate events were merged. Besides, events that were shorter than 400 ms or have fewer than three spike-wave cycles were excluded from the SWD collection. The threshold value was adjusted by eye inspection for each mouse based on a sample file until no true positive events were excluded and most false events rejected. Between individual mice this threshold varied between 4.2 – 6.9 SD in WT and 2.7-5.0 SD in APP/PS1 mice. In the final step, we used a customized user interface to help an experience human rater blinded to the mouse genotype decide

the acceptance vs. rejection of each candidate event based on the regularity of the spike-wave pattern. The number of SWD events in each genotype and at two ages was counted and divided by the total time of immobility (i.e. waking immobility+ NREM). The data were analyzed by two-way ANOVA with genotype and age as factors.

Pre-SWD power at 2 - 4 Hz range (Lüttjohann et al., 2013), 5 - 9/ 6 -12 Hz range (Lüttjohann et al., 2013; Pinault et al., 2001), and 20-40 Hz range (Sorokin et al., 2016) have been reported to positively correlate with spontaneous SWD events in a genetic absence-epilepsy rat model. To test if this is the case in our WT and APP/PS1 mice (middle-aged mice only), we screened out all SWD events that occurred at least 60 s after the end of the previous SWD event, and then divided the preceding 60-s epochs into 2-s bins. To test whether SWDs associate with slow fluctuations in above mentioned frequencies, we compared the PSD in latter and earlier half of the 60-s epoch preceding the SWDs with paired t-test. Besides, to determine the association between SWDs and these power ranges in a smaller time scale, we compared the 2-4 Hz, 6-12 Hz or 20-40 Hz power between adjacent 2-s bins across the 60 s preceding the SWD by using paired t-test.

To search for the amplitude modulation by oscillation phase in the middle-aged mice, we first plotted the bispectrum of raw data, which indicates interacting frequency triplets (Kramer et al., 2008). Based on the bispectrum, we chose to examine (1) delta (2–4 Hz) phase/gamma (40–100 Hz) amplitude modulation and (2) theta (6–10 Hz) phase/gamma (40–100 Hz) amplitude modulation. In order to quantify the extent of modulation, we estimated the modulation index (MI) based on a normalized entropy measure, as described previously (Gurevicius et al., 2013; Tort et al., 2008). The higher the MI value, the stronger is the cross-frequency coupling (amplitude-phase) between two frequency ranges of interest. We estimated the mean power of gamma oscillation for each 1 Hz bin. Statistical significance of MI was estimated by creating shuffled data of the time series (phase of one sweep and amplitude of another) and generated 200 surrogate MI values, from which each MI value was calculated from 20 random pairs. Assuming a normal distribution of the surrogate MI values, a significance threshold was then calculated by using $p < 0.01$ as the threshold. All comparisons were done using Friedman's test due to the lack of normal distribution of MI values and unpaired sizes of samples in each comparison group.

2.6 AEP data analysis

In the paired-pulse auditory stimulus experiment the AEPs in the frontal cortex showed constantly two components at 20 (N1) and 30 (P1) ms after the click stimulus in all tested mice. First, the baseline was corrected for each mouse by averaging background EEG between 0 and 100 ms before the stimulus onset. The amplitude of each peak or trough was the difference between the absolute maximum and the baseline level, while the peak latency was calculated from the stimulus onset. When estimating habituation of the AEP (auditory gating), we first calculated the amplitude difference between the N1 and P2 peaks as described previously (Bickford-Wimer et al., 1990). Then paired-pulse ratios were calculated for the P2 – N1 difference by dividing the response amplitude after the second stimulus (A2, test stimulus) by the response amplitude after the first stimulus (A1, conditioning stimulus) and further converted the ratio into percentage (ratio = A2/A1 × 100%). Peak latency was defined as the time of peak (or trough) from the onset of sound stimuli. The data from the two genotypes and two ages were compared using two-way ANOVA with the genotype and age as factors. In all analyses, the threshold for significance was set to 0.05. The results are presented as means ± SEM.

2.7 Acoustic startle response and pre-pulse inhibition

The acoustic startle response to the presentation of a sudden loud sound is a sensitive indicator of the general reactivity of an animal. Pre-pulse inhibition, i.e., reduction of the startle response to the sudden loud sound by a weak preceding sound pulse, is a sensitive measure of slow inhibitory mechanisms and closely related to the auditor gating of AEPs. The startle response system (TSE-Systems, Bad Hamburg, Germany) comprised a sound-attenuation chamber (39 cm x 38 cm x 58 cm) and a highly sensitive scale located between two loudspeakers. The mouse was placed in a restrainer (4.5 cm x 9 cm x 4.5 cm) on top of the scale. The startle response was measured as an apparent weight increase-decrease due to muscle contractions. The mouse was first exposed for 5 min to background white noise (65 dB) that remained on during the testing. A startle pulse (40 ms, 110 dB) was presented alone or preceded with a pre-pulse stimulus (20 ms) at three intensities (20, 35, 50 dB). The time between the pre-pulse and the startle pulse was 220 ms. The inter-trial interval varied randomly between 20 and 25 s. Each condition was presented 12 times, and the median response to each pre-pulse was taken into further analysis. To quantify spontaneous motor twitches independent of external stimulation (as a proxy for myoclonus), we let the mice stay in the system for 20 min and counted all startles with an ostensible weight exceeding 10.0 g. The study group (9 female APP/PS1 mice and 8 WT littermates) were recorded at 3, 7 and 11 months of age. The body weight was taken at each age before the recording. The statistical analysis of the startle responses

was done with ANOVA for repeated measures, with the age as within-subject and the genotype as between-subject factor.

3. Theory

This work compares APP/PS1 transgenic mice to their wild-type (WT) controls at a 'symptomatic' age (14-16 months) of AD-like brain amyloidosis and uses our previously published data on 4-month-old ('pre-symptomatic', pre-plaque) APP/PS1 and WT mice as reference. EEG parameters that reflect general aging should not show up as difference between APP/PS1 and WT mice. Those parameters that reflect the influence of soluble Aβ species or other APP breakdown products should differentiate APP/PS1 and WT mice to the same extent at the two ages or less at middle ages than young adult age. In contrast, parameters that reflect the effect of progressive brain amyloidosis with plaque formation and plaque-associated inflammatory and degenerative changes should show up as difference between the genotypes at 14-16 months of age but not at the younger age.

4. Results

4.1 Increased power spectral density over beta – gamma frequencies in middle-aged APP/PS1 mice

Using the same recording methods and protocol as in our previous study on 4-month-old APP/PS1 mice (Gurevicius et al., 2013) we collected data from 14 APP/PS1 and 16 wild-type littermate mice at the age of 14-16 months. Figure 1 illustrates the histologically verified electrode locations and the extent of amyloid plaque pathology in each site at the end of the recordings. Supplementary Table 1 summarizes the number of mice with given electrode location used in the final analysis. We compared the EEG/LFP power spectral density between genotypes in seven brain regions, medial and superficial frontal cortex (mFC/sFC), parietal cortex (PC), dentate gyrus (DG), lateral geniculate nucleus of thalamus (TH), and superficial and deep visual cortex (sVC, dVC), under movement, waking immobility and NREM sleep states (no REM was detected). Across all behavioral states, the power spectral density of both genotypes revealed two peaks, one in theta-band (5-9 Hz) and another in a narrow gamma band (40-80 Hz). However, mFC showed a peak in the delta-band (1-4 Hz) during waking immobility and NREM sleep (Fig. 2). In addition, the APP/PS1 mice showed a peak at 15-30 Hz window during waking immobility and NREM sleep, most prominent at the sFC, PC and dVC electrodes (Fig. 2).

To compare the power spectral densities between the genotypes, we separated the brain regions and behavioral states and ran multiple t-tests for each 1 Hz bin using false discovery rate correction for multiple comparisons (Benjamini and Hochberg, 1995). Except for movement in mFC and all behavioral states in TH and sVC, APP/PS1 mice showed a significant power increase compared to WT mice (Fig. 2). The power enhancement in sFC and PC ranged 8-110 Hz, in DG covered 7-25 Hz, whereas mFC and dVC showed a narrower power increase at 12-28 Hz.

4.2 Increased alpha-beta power in APP/PS1 mice during NREM sleep is age-independent

At first glance, the difference in cortical power spectral density between middle-aged APP/PS1 and WT mice appears similar as what we earlier reported in young adult mice (Gurevicius et al., 2013). However, to better compare the present results with the published ones, reanalyzed the previous data together with the present data for the sFC channel and NREM state where the genotype difference was the largest. To this end, we divided the PSD into conventional frequency bands, delta (1-4 Hz), theta (5-9 Hz), alpha (10-15 Hz), beta (16 – 29 Hz), and gamma (30 – 100 Hz) and compared the power in these bands between the old dataset on young mice and the present one on middle-aged mice. Since a different amplifier was used in these two studies, we normalized the total power to be same in the WT mice of two ages. This comparison showed a significant increase in theta ($F_{1,43} = 11.5$, $p = 0.001$), alpha ($p < 0.001$) and beta ($p < 0.001$) power in APP/PS1 mice compared to WT littermates independent of age (Fig. 3). In contrast, there was a significant age-related increase in gamma power in WT but not in APP/PS1 mice (Fig. 3), resulting in significant age x genotype interaction ($F_{1,43} = 12.0$, $p = 0.001$), and no significant changes in the delta power.

4.3 Spike-wave discharge events associate with increased cortical beta power

Next, we explored more closely the contributing components to the extra peak at 12-25 Hz that was present only in APP/PS1 mice during waking immobility and NREM sleep (Fig. 2) concentrating on the sFC channel with the most prominent peak in this range. This investigation in APP/PS1 mice revealed numerous discharge complexes that resembled classic spike-wave discharges (SWDs) in genetic rat models of absence epilepsy (Coenen et al., 1991; Vergnes et al., 1987). These were short (0.4 – 3s) bursts of activity, occurring symmetrically on the screw electrodes over the fronto-parietal cortex, but being totally absent in medial frontal cortex and absent or less clearly structured in the visual cortex (Fig. 4A). In the thalamus (Po nucleus), a synchronized oscillation of opposite

polarity was observed (Fig. 4B). The basic frequency of these SWDs was between 7-10 Hz with additional peaks in the 12-25 Hz range (Fig. 4B,D). As in rat models of absence seizures, the SWDs were most frequent during quiet wakefulness and light NREM sleep, but absent during movement or REM sleep (Coenen et al., 1991). Often the SWD event ended with a small head movement, which showed up as a high-frequency EMG artifact on the cortical screw channel (Fig. 5A).

We further determined the frequency of occurrence of SWDs in APP/PS1 vs. WT littermates at 4-5 months and 14-16 months of age. Since SWDs occurred only during immobility, whereas the time of movement varied between individual mice, we calculated the number of SWDs per hour of immobility. Independent of age, we detected ~15 times more SWDs in middle-aged and ~5 time more SWDs in young APP/PS1 mice than in their WT littermates (genotype: $F_{1,39} = 23.8$, $p < 0.001$; Fig. 5B). The mean duration of SWDs decreased with age ($F_{1,39} = 34.5$, $p < 0.001$), and was higher in APP/PS1 mice ($p < 0.001$). However, the genotype difference in SWD duration became smaller with age (age x genotype interaction, $p = 0.01$).

Calculating the envelope covering most of the frequencies in the SWD events, from 7 to 23 Hz, helped us to detect those events (Fig. 5A). However, after cutting the SWD events off from the raw EEG recordings, we found that the waking immobility and NREM associated PSD 12-25 Hz peak of cortical screw channels in APP/PS1 mice was only marginally reduced (Fig. 5C). This implies that the major proportion of increased beta power in APP/PS1 mice arises from more long-lasting oscillations than SWD events.

4.4 SWDs are preceded by an increase in PSD in 6-12 Hz and 20 – 40 Hz ranges

Several papers have reported that SWDs in the genetic rat models of absence epilepsy are preceded by an increased in the background EEG power. However, the specific frequency range of increases varies between the studies, including delta (2-4 Hz; Lüttjohann et al., 2013), theta (5-9/ 6-12 Hz) range (Lüttjohann et al., 2013; Pinault et al., 2001) and 20-40 Hz range (Sorokin et al., 2016). These findings urged us to investigate if a similar relationship holds for increased delta-theta and 20-40 Hz power vs. occurrence of SWDs in middle-aged APP/PS1 mice. To this end, we divided the 60-s epochs preceding single SWDs in 2-s bins and compared 2-4 Hz + 6-12 Hz, 6- 12 Hz, and 20-40 Hz power in each bin to the preceding one. In both APP/PS1 (240 epochs) and WT mice (56 epochs), we found a significant increase in the bin immediately preceding the SWD for the 6-12 Hz range alone or combined with 2-4 Hz (Fig. 6). Moreover, the averaged power during the latter half of the 60-s epoch preceding the SWD was significantly higher than in the earlier half for the 20 – 40 Hz in

both APP/PS1 and WT mice, and for 6 – 12 Hz in the APP/PS1 mice (Fig. 6). These findings are thus consistent with findings in genetic rat models of absence seizures. Further, they suggest that the increase in 15 – 25 Hz power seen in the PSD spectrum may indeed arise from this ~ 30 s pre-ictal pattern.

4.5 Nested theta-gamma and delta-gamma oscillations are intact in APP/PS1 mice

Our finding of increased cortical and hippocampal power within the gamma range led us to study more closely the time of occurrence of gamma oscillation and especially their modulation by lower frequency oscillations. Since nested hippocampal theta-gamma oscillations have been found to associate with memory and decision making (Tort et al., 2009, 2008), these were of our particular interest. In addition, we found a robust delta phase/ gamma amplitude coherence in mFC (Fig. 7 AB) that to our knowledge has not been reported in the mouse before. To this end, we first calculated bicoherence (Kramer et al., 2008) in every brain region - behavioral state pair, and found strong delta-gamma coherence in mFC and theta-gamma in DG (Fig. 7,8). To quantify the extent the nested oscillations interact, we measured a Modulation Index (Gurevicius et al., 2013; Tort et al., 2008). The index for delta (2–4 Hz) phase/gamma (40–100 Hz) amplitude co-modulation in mFC was significantly higher than shuffled data during waking immobility and NREM sleep (Fig. 7C). Another, less prominent delta/gamma co-modulation was observed in DG during NREM (Fig. 7C). In mFC, the Modulation Index differed significantly only between the behavioral states ($p < 0.01$ and $p < 0.001$, Friedman's test; Fig. 7D), while in DG, a genotype-dependent difference was additionally discovered during NREM sleep ($p < 0.01$; Fig. 7D). When applying the same analysis to theta (5–9 Hz) phase/ gamma (40–100 Hz) amplitude, a strong co-modulation was revealed in mFC, DG, TH and dVC ($p < 0.05$, $p < 0.01$ and $p < 0.001$, respectively; Fig. 8C). Co-modulation in DG and dVC differed significantly between behavioral states ($p < 0.05$ and $p < 0.01$), while in mFC and TH no difference was detected either between the behavioral states or the genotypes. Thus, the finding of behavioral state dependent but genotype independent theta-gamma co-modulation in middle-aged APP/PS1 mice corroborates findings in 4-month-old APP/PS1 mice (Gurevicius et al., 2013).

4.6 Abnormal AEPs in middle-aged APP/PS1 mice

Besides increased cortical and thalamic PSD power over a broad frequency range, our previous

study in young adult APP/PS1 mice revealed increased amplitude of auditory evoked potentials (AEPs), which also speaks for increased neuronal excitability in these mice (Gurevicius et al., 2013). We were interested in seeing whether this AEP enhancement persists until middle ages. In addition, we employed the auditory gating paradigm with paired brief tones to assess long-latency inhibition in the auditory cortex. Typically, the response to the second (test) stimulus is dramatically attenuated compared to the first (conditioning) one, with a maximum reduction at 500 ms inter-stimulus interval (Bickford-Wimer et al., 1990). Such a long interval likely involves sustained $GABA_B$-mediated mechanisms (Hershman et al., 1995). The cortical AEPs of both APP/PS1 and WT mice had two main components, N1 and P2 (Fig. 9A). To better evaluate the aging-related change in these AEPs parameter between APP/PS1 and WT mice, we reanalyzed the data from young adult mice (Gurevicius et al., 2013) together with the present results. As the PSD was normalized to be equal between young and aged WT mice, we took the square (amplitude vs. power) of this correction factor to adjust the AEP amplitudes. Since this is only an estimate the absolute power differences can be only considered suggestive. However, the latency and auditory gating (P2-N1 habituation) are measures that are independent of the absolute power, and thus fully comparable between to data sets. The N1 amplitude response to the conditioning tone did not show a significant genotype difference ($F_{1,42} = 3.2$, $p = 0.08$), but the P2 amplitude triggered by the conditional stimulus was significantly higher in APP/PS1 mice than in WT mice independent of age ($F_{1,42} = 10.4$, $p = 0.002$). The N1 latency increased with age in both WT and APP/PS1 mice ($F_{1,42} = 25.7$, $p < 0.001$) but that of P2 remained unchanged ($p = 0.14$; Fig. 9B). In contrast, auditory gating did not differ between the genotypes (all ps > 0.49; Fig. 9C).

4.7 Acoustic and spontaneous startles are more common in young adult APP/PS1mice than in wild-type littermates

As a behavioral manifestation of reactivity to paired brief tones we tested the acoustic startle responses to a 110 dB white noise with prepulses of varying intensity at 3, 7 and 11 months of age in a separate cohort of mice. At all ages, the startle amplitude decreased with an increasing sound level of the prepulse ($F_{3,45} = 3.9 – 12.8$, $p < 0.01$), and there was no prepulse sound level x genotype interaction ($p > 0.13$). Importantly, the acoustic startle response was larger in APP/PS1 mice than in wild-type littermates at 3 months of age ($F_{3,17} = 12.3$, $p = 0.003$; Fig. 10A) and at 7 months ($F_{3,16} = 5.9$, $p = 0.03$; Fig. 10B), but no longer at 11 months ($F_{3,15} = 1.0$, $p = 0.33$; Fig. 10C).

To further assess whether APP/PS1 mice have signs of myoclonus, we recorded spontaneous startles during 20 min in a sound-attenuated chamber. There was a general increase in the suprathreshold startles (Fig. 10D) with age, but that can be largely ascribed to increase in body weight (Fig. 10E). Importantly, there was a main effect of genotype ($F_{1,15} = 11.8$, $p = 0.004$) and a significant age x genotype interaction ($F2_{,30} = 8.4$, $p < 0.001$), such that APP/PS1 mice show more spontaneous startles than wild-type littermates at 3 and 7 months of age but no longer at 11 months of age. Collectively, these findings suggest that both the enhanced spontaneous muscle jerks and sound provoked behavioral reactivity of APP/PS1 mice decline toward normal levels by 12 months of age.

4.8 Sudden deaths of APP/PS1 mice show a peak in early adulthood

Finally, to see whether age-dependent decline in startle reactivity also reflects sudden deaths in APP/PS1 mice, we went through the records of our breeding colony for 656 $APP_{Swe}/PS1_{dE9}$ mice that were not sacrificed for sampling before the age of 12 months (the usual age for cognitive testing). We found 82 records (12.5 %) of spontaneous preterm deaths. As illustrated in Supplementary Figure S1, the distribution of ages at death was strongly skewed, with a peak around 2 months and mean at 3.2 months of age. Very few sudden deaths were observed after 6 months of age.

5. Discussion

The present study demonstrated that EEG/LFP signatures of increased cortical excitability found in amyloid plaque producing APP/PS1 mice at 4 months of age persisted beyond middle age. Increased cortical power in high-theta, alpha and beta frequencies were elevated in APP/PS1 independent of age, while the elevation in low-gamma band found in 4-month-old APP/PS1 mice tended to subside by 14-16 months. In both young and middle-aged APP/PS1 this increase in cortical power was accompanied by frequent spike-wave discharges (SWDs), which have been

largely overlooked in earlier EEG studies on APP transgenic mice, including our own (Gurevicius et al., 2013; Wang et al., 2002). In addition, the hippocampal LFPs showed significantly increased power at 7-25 Hz in middle-aged APP/PS1 mice, which was not seen at 4 months of age. Further, augmented auditory evoked potential seen in 4-month-old APP/PS1 mice were also present in middle-age APP/PS1 mice. These electrophysiological signatures of maintained increased excitability in forebrain structures with amyloid pathology in APP/PS1 mice are in striking contrast with the normalization of acoustic and spontaneous startles, which are mainly dependent on brainstem circuits (Swerdlow et al., 2001).

Essentially, increased cortical EEG power from 7 Hz up to ~60 Hz that we earlier reported in 4-month-old $APP_{Swe}/PS1_{dE9}$ mice (Gurevicius et al., 2013) was still present at the age of 14-16 months. Only the high-gamma (70 – 100 Hz) tended to normalize in APP/PS1 mice with age. On the other hand, increased power from 10 – 30 Hz in the hippocampus became significant in APP/PS1 mice compared to WT mice only in the middle-aged mice. This would correspond to the progression of amyloid plaque pathology that, as in the case of human disease, in more advanced in the frontal and parietal cortex than in the hippocampus (Minkeviciene et al., 2008). Of note, there was a specific augmentation of cortical power at 12 – 25 Hz in APP/PS1 mice at both 4 and 14-16 months of age. This increase in beta power appears to be the most consistent finding in APP transgenic mice (Gurevicius et al., 2013; Jyoti et al., 2010; Wang et al., 2002), and one previous study suggested that beta power (recorded up to 20 Hz) may increase with age (Jyoti et al., 2010). A selective increase in cortical 20-30 Hz beta oscillation is a characteristic EEG change in hemiparkinsonian 6-OHDA rats (Sharott et al., 2005) and raises the question whether APP transgenic mice show striatal dopamine depletion with age. At least as far as the $APP_{Swe}/PS1_{dE9}$ mouse is concerned, middle-aged mice of this line have no reported decline in striatal dopamine contents and only modest functional impairment in stimulated striatal dopamine release (Kärkkäinen et al., 2015; Perez et al., 2005). Further, the 6-OHDA model displays increased beta power only in the motor cortex while we found it even in the visual cortex (Fig. 2). On the other hand, a recent study employing optogenetics demonstrated that specific stimulation of striatal cholinergic interneurons in young adult mice results in increased power of oscillations from 8 to 100 Hz but not of lower frequencies (Kondabolu et al., 2016). Despite striking similarity to observed increase in cortical power in APP/PS1, this mechanisms is difficult to reconcile with previous studies in $APP_{Swe}/PS1_{dE9}$ mice revealing decreased ACh release in striatal slices already at 6 months of age (Machová et al., 2010). A third mechanism that has been described to increase cortical beta-oscillations is manipulation of GABA receptors. $GABA_A$ antagonists increase cortical

beta-gamma power (maximum 20-30 Hz) in freely moving rats (Van Lier et al., 2004). Indeed, acute application of Aβ has been shown to inhibit GABA neurotransmission by downregulation of $GABA_A$ receptors (Ulrich, 2015). In addition, diminished density of perisomatic GABAergic (typically $GABA_A$ subtype) nets has been reported around cortical amyloid plaques in $APP_{Swe}/PS1_{dE9}$ mice (Garcia-Marin, 2009) and in vivo imaging revealed spontaneous hyperactivity of neurons around amyloid plaques in another APP/PS1 mouse (Busche et al., 2008). No study so far has specifically studied changes in $GABA_B$ receptors in amyloid plaque forming mice. However, the present finding of intact auditory gating in middle-aged APP/PS1 mice despite general augmentation of AEPs is consistent with the idea of preserved $GABA_B$ signaling (Hershman et al., 1995) combined with impaired short-latency inhibition via $GABA_A$ receptors.

The present study revealed a high prevalence of SWDs in APP/PS1 mice independent of age. SWDs have been well characterized in genetic rat models of absence seizure, such as Wistar-derived inbred lines WAG/Rij (Russo et al., 2016) and GAERS (Depaulis et al., 2016). However, SWD duration in the models is typically much longer, on average 7 s for WAG/Rij (Lüttjohann et al., 2013) and 25 s for GAERS rats (Depaulis et al., 2016), than what we found in the APP/PS1 mice (0.5 – 3 s). This raises the question whether these are after all comparable. Namely, 0.5 – 3 s short bouts of medium amplitude 5-9 Hz activity have been reported to precede longer and more prominent SWDs in GAERS rats (Pinault et al., 2001). Further, WAG/Rij rats show two types SWDs. Besides the about 7-s long typical SWDs that are recorded bilaterally over the entire cortex with a maximum over the somotomotor cortex, they also show ~1.5-s long SWDs of lower basic frequency (5.5 – 7 Hz) often restricted to only one hemisphere and parieto-occipital cortex (Midzianovskaia et al., 2001).

Nevertheless, except for the shorter duration, the SWDs we have recorded in APP/PS1 mice well correspond to typical SWDs in the rat models of absence epilepsy. The SWDs are preceded by increased cortical power in theta and beta frequencies for about 30 s, they show the typical spike-wave structure with a basic frequency at 7-10 Hz and surface negative spikes, and they are always bilateral with a maximum over the frontal and parietal convexity and much less clear in the occipital cortex and absent in the medial frontal cortex (Vergnes et al., 1987). Further, they are accompanied by SWDs in the Po and RT (our unpublished observation) thalamic nuclei that are opposite in polarity and synchronized to cortical SWDs. Moreover, the average duration of inbred mouse lines considered models of absence seizures have an average duration of SWDs between 0.6 – 3 s (Letts

et al., 2014). Collectively, these findings suggest that APP/PS1 mice with SWDs share a lot of similarity to established rodent models of absence seizures.

Spontaneous seizures described in amyloid plaque forming transgenic mice are typically longer than 10 s, followed by post-ictal EEG suppression, and often associated with myoclonus or convulsions (Minkeviciene et al., 2009; Palop et al., 2007; Westmark et al., 2010). In contrast, classic SWDs have been quantified or even mentioned in few reports. Nevertheless, these cover four very different mouse models carrying APP mutations, $APP_{Swe}/PS1_{dE9}$ (Nygaard et al., 2015; Zilberter et al., 2013), $APP_{Swe,Ind}$ (Hazra et al., 2016); APP_{Arc} (Ziyatdinova et al., 2016), and 3xTg ($APP_{Swe}/PS1_{M146V}$ (Nygaard et al., 2015), and therefore cannot be just manifestation of some mouse line specific feature.

The finding of frequent SWDs specifically in amyloid plaque forming mice is intriguing because the underlying circuitries and neurotransmission of SWDs has been intensively studied over the past three decades and may provide a clue to the link between amyloid pathology and SWDs. Although opinions about the trigger site of SWDs are still divided, the current consensus is that especially the somatosensory cortex, VP, Po, and RT thalamic nuclei are intimately involved in these oscillations (Meeren et al., 2005). Somatosensory cortex is among the sites of first amyloid accumulation in the $APP_{Swe}/PS1_{dE9}$ mouse (Garcia-Alloza et al., 2006), and GABAergic perisomatic nets are diminished around neurons near amyloid plaques in these mice (Garcia-Marin et al., 2009), leading to reduced $GABA_A$ergic inhibition as found in WAG/Rij rats (Russo et al., 2016). On the other hand, a similar heavy amyloid plaque load is seen in medial frontal cortex that did not show any SWDs in our mice, suggesting that increased local cortical excitability is not sufficient to trigger an SWD. Besides reduced $GABA_A$ activity in the cortex, an imbalance between $GABA_A$ and $GABA_B$ inhibition in the thalamus has been suggested to play a key role in the generation of SWDs (Beenhakker and Huguenard, 2009; Russo et al., 2016). The thalamus is not the primary site for amyloid plaque formation in amyloid plaque forming transgenic mice, but our APP/PS1 do express scattered amyloid plaques in the thalamus from 5 months on (Minkeviciene et al., 2009). Astrogliosis around the plaques likely release GABA extrasynaptically in the thalamus as shown for hippocampus (Jo et al., 2014), and extrasynaptic GABA-receptors in the ventrobasal thalamus are predominantly of the $GABA_B$ type (Kulik et al., 2002). Further, since $GABA_B$ receptor activation at reticular neurons requires a stronger input than $GABA_A$ receptor activation (Beenhakker and Huguenard, 2009), increased excitability of cortico-thalamic projection neurons due to advanced amyloid plaque pathology in the cortex may translate to altered $GABA_A$ vs. $GABA_B$ balance at

reticular nucleus. On the other hand, a recent study found in the $APP_{Swe,Ind}$ mouse impaired cortical input selectively to reticulate thalamic nucleus (Hazra et al., 2016), demonstrating another potential source of imbalance in the cortico-thalamic and intrathalamic circuitry. SWDs in APP/PS1 mice also closely resemble high-amplitude EEG bursts found in aged Wistar rats, known as high-voltage spindles in earlier literature (Buzsáki et al., 1988). These can be induced in young adult rats by lesioning the cholinergic nucleus basalis (Riekkinen et al., 1990), and in aged rats treatment with cholinesterase inhibitors reduce their occurrence (Riekkinen et al., 1991). The $APP_{Swe}/PS1_{dE9}$ mouse shows significantly blunted cortical cholinergic neurotransmission already at 7 months of age and further progression of the impairment to 17 months (Machová et al., 2008), which suggest that reduced cholinergic tone may be one of the underlying factor for SWDs. In addition, lesioning the ascending noradrenergic pathways to the cortex induces SWDs in rats (Riekkinen et al., 1992), and this can be reversed by α2-adrenoreceptor antagonists (Jäkälä et al., 1992). Whether this effect is direct on SWD generation or indirect through changing the overall state of vigilance to favor SWD occurrence remains open, but interestingly APPswe/PS1dE9 mice show a dramatic age-dependent decline in the cortical and hippocampal noradrenergic innervation, which may also contribute to SWDs. Taken together, several changes associated with progressive amyloid pathology and aging render the APP/PS1 susceptible for SWDs and await further studies to reveal the exact underlying mechanisms.

Since the first attempts to generate amyloid plaque producing mice, sudden deaths of unknown reasons have plagued the breeding colonies of APP transgenic mice (Carlson et al., 1997; Hsiao et al., 1995; Roberson et al., 2007). It looks like Aβ formation plays a key role in early mortality, since human wild-type APP overexpression is less lethal than overexpression of Aβ producing mutant APP forms (Carlson et al., 1997). On the other hand, the early mortality is highly dependent on the genetic background (Carlson et al., 1997; Hsiao et al., 1995), and can be alleviated by knocking out microtubulus associated protein tau gene (Roberson et al., 2007). Our breeding colony statistics clearly indicate that sudden deaths peak at 2-3 months of age in $APP_{Swe}/PS1_{dE9}$ mice. The only other published colony statistics found a similar peak between 3.5 – 5.5 months in $APP_{Swe,Ind}$ (J20) mice (Roberson et al., 2007) and no mortality between 6 and 12 months of age. Interestingly, amyloid plaque formation begins around 4 months of age in APP_{Swe}/PS1dE9 mice and at 5-6 months of age in $APP_{Sw,Ind}$ (J20) mice (Mucke et al., 2000). Thus, the majority of sudden deaths takes place before amyloid plaque formation. In parallel with decreasing risk of sudden death, startle responses to loud sound or spontaneous startles tended to decrease in APP/PS1 mice to the

levels of their wild-type littermates. It is possible that both sudden deaths and increased startles responsiveness reflect a brainstem-level pathology associated with increased levels of soluble Aβ.

To conclude, comparison of young adult and middle-aged APP/PS1 mice demonstrate that EEG signs of cortical hyperexcitability, including increased cortical power over 8 – 60 Hz, frequent SWDs and enhance auditory evoked potentials compared to wild-type littermates persist until middle ages. In contrast, sudden deaths and enhanced startle reflexes gradually disappear with aging. The different time course of these two phenomena related to neuronal hyperexcitability speaks for different underlying mechanisms. Further, they are mediated by different circuitries, thalamo-cortical vs. brainstem networks, with only the thalamo-cortical circuitry significantly affected by amyloid pathology. Since the circuitry underlying SWDs is limited to certain thalamic nuclei and neocortical areas and the generation of SWDs is relatively well characterized, SWDs in APP transgenic mice present a promising new model to investigate molecular and cellular mechanisms associated with amyloid pathology. In addition, since they are easily recorded with only epidural electrodes and remain constant over months according to our experience, they provide an outstanding biomarker for preclinical intervention studies. There is limited evidence that the high number of SWDs in APP transgenic mice also associate with memory impairment (Nygaard et al., 2015). More direct studies are needed to assess the relationship between SWDs and memory or attentional impairment, but if this relationship holds true, SWDs are also interesting candidates for rapidly fluctuating changes in cognition in patients with Alzheimer's disease or Lewy body disease.

Acknowledgements

This work was supported by grants from the following foundations: Sigrid Juselius Foundation (Finland), Olav Thon Foundation (Norway), Finnish Cultural Foundation.

Disclosure

None of the authors have conflicting financial interest related to the manuscript

References

Beenhakker, M.P., Huguenard, J.R., 2009. Neurons that Fire Together Also Conspire Together: Is Normal Sleep Circuitry Hijacked to Generate Epilepsy? Neuron. https://doi.org/10.1016/j.neuron.2009.05.015

Benjamini, Y., Hochberg, Y., 1995. Controlling the false discovery rate: a practical and powerful approach to multiple testing. J. R. Stat. Soc. B. https://doi.org/10.2307/2346101

Bickford-Wimer, P.C., Nagamoto, H., Johnson, R., Adler, L.E., Egan, M., Rose, G.M., Freedman, R., 1990. Auditory sensory gating in hippocampal neurons: A model system in the rat. Biol. Psychiatry 27, 183–192. https://doi.org/10.1016/0006-3223(90)90648-L

Born, H.A., Kim, J.-Y., Savjani, R.R., Das, P., Dabaghian, Y.A., Guo, Q., Yoo, J.W., Schuler, D.R., Cirrito, J.R., Zheng, H., Golde, T.E., Noebels, J.L., Jankowsky, J.L., 2014. Genetic Suppression of Transgenic APP Rescues Hypersynchronous Network Activity in a Mouse Model of Alzeimer's Disease. J. Neurosci. 34, 3826–3840. https://doi.org/10.1523/JNEUROSCI.5171-13.2014

Busche, M.A., Eichhoff, G., Adelsberger, H., Abramowski, D., Wiederhold, K.-H., Haass, C., Staufenbiel, M., Konnerth, A., Garaschuk, O., 2008. Clusters of hyperactive neurons near amyloid plaques in a mouse model of Alzheimer's disease. Science 321, 1686–9. https://doi.org/10.1126/science.1162844

Buzsáki, G., Bickford, R.G., Armstrong, D.M., Ponomareff, G., Chen, K.S., Ruiz, R., Thal, L.J., Gage, F.H., 1988. Electric activity in the neocortex of freely moving young and aged rats. Neuroscience 26, 735–744. https://doi.org/10.1016/0306-4522(88)90095-4

Carlson, G.A., Borchelt, D.R., Dake, A., Turner, S., Danielson, V., Coffin, J.D., Eckman, C., Meiners, J., Nilsen, S.P., Younkin, S.G., Hsiao, K.K., 1997. Genetic modification of the phenotypes produced by amyloid precursor protein overexpression in transgenic mice. Hum. Mol. Genet. 6, 1951–9. https://doi.org/10.1093/HMG/6.11.1951

Coenen, A.M.L., Drinkenburg, W.H.I.M., Peeters, B.W.M.M., Vossen, J.M.H., van Luijtelaar, E.L.J.M., 1991. Absence epilepsy and the level of vigilance in rats of the WAG/Rij strain. Neurosci. Biobehav. Rev. https://doi.org/10.1016/S0149-7634(05)80005-3

Corbett, B.F., Leiser, S.C., Ling, H.-P., Nagy, R., Breysse, N., Zhang, X., Hazra, A., Brown, J.T., Randall, A.D., Wood, A., Pangalos, M.N., Reinhart, P.H., Chin, J., 2013. Sodium channel cleavage is associated with aberrant neuronal activity and cognitive deficits in a mouse model of Alzheimer's disease. J. Neurosci. 33, 7020–6. https://doi.org/10.1523/JNEUROSCI.2325-12.2013

Depaulis, A., David, O., Charpier, S., 2016. The genetic absence epilepsy rat from Strasbourg as a model to decipher the neuronal and network mechanisms of generalized idiopathic epilepsies. J. Neurosci. Methods. https://doi.org/10.1016/j.jneumeth.2015.05.022

Dickerson, B.C., Salat, D.H., Greve, D.N., Chua, E.F., Rand-Giovannetti, E., Rentz, D.M., Bertram, L., Mullin, K., Tanzi, R.E., Blacker, D., Albert, M.S., Sperling, R.A., 2005. Increased hippocampal activation in mild cognitive impairment compared to normal aging and AD. Neurology 65, 404–411. https://doi.org/10.1212/01.wnl.0000171450.97464.49

Garcia-Alloza, M., Robbins, E.M., Zhang-Nunes, S.X., Purcell, S.M., Betensky, R.A., Raju, S., Prada, C., Greenberg, S.M., Bacskai, B.J., Frosch, M.P., 2006. Characterization of amyloid deposition in the APPswe/PS1dE9 mouse model of Alzheimer disease. Neurobiol. Dis. https://doi.org/10.1016/j.nbd.2006.08.017

Garcia-Marin, V., 2009. Diminished perisomatic GABAergic terminals on cortical neurons adjacent to amyloid plaques. Front. Neuroanat. 3. https://doi.org/10.3389/neuro.05.028.2009

Gurevicius, K., Lipponen, A., Tanila, H., 2013. Increased cortical and thalamic excitability in freely moving APPswe/PS1dE9 mice modeling epileptic activity associated with alzheimer's disease. Cereb. Cortex 23, 1148–1158. https://doi.org/10.1093/cercor/bhs105

Hämäläinen, A., Pihlajamäki, M., Tanila, H., Hänninen, T., Niskanen, E., Tervo, S., Karjalainen, P.A., Vanninen, R.L., Soininen, H., 2007. Increased fMRI responses during encoding in mild cognitive impairment. Neurobiol. Aging 28, 1889–1903. https://doi.org/10.1016/j.neurobiolaging.2006.08.008

Hazra, A., Corbett, B.F., You, J.C., Aschmies, S., Zhao, L., Li, K., Lepore, A.C., Marsh, E.D., Chin, J., 2016. Corticothalamic network dysfunction and behavioral deficits in a mouse model of Alzheimer's disease. Neurobiol. Aging 44, 96–107. https://doi.org/10.1016/j.neurobiolaging.2016.04.016

Hershman, K.M., Freedman, R., Bickford, P.C., 1995. GABAB antagonists diminish the inhibitory gating of auditory response in the rat hippocampus. Neurosci. Lett. 190, 133–136. https://doi.org/10.1016/0304-3940(95)11523-Y

Hsiao, K.K., Borchelt, D.R., Olson, K., Johannsdottir, R., Kitt, C., Yunis, W., Xu, S., Eckman, C., Younkin, S., Price, D., Iadecola, C., Clark, H.B., Carlson, G., 1995. Age-related CNS disorder and early death in transgenic FVB/N mice overexpressing Alzheimer amyloid precursor proteins. Neuron 15, 1203–1218. https://doi.org/10.1016/0896-6273(95)90107-8

Ittner, A.A., Gladbach, A., Bertz, J., Suh, L.S., Ittner, L.M., 2014. p38 MAP kinase-mediated NMDA receptor-dependent suppression of hippocampal hypersynchronicity in a mouse model of Alzheimer's disease. Acta Neuropathol. Commun. 2. https://doi.org/10.1186/s40478-014-0149-z

Jäkälä, P., Viitamaa, T., Sirviö, J., Riekkinen, P., Salonen, J., Haapalinna, A., Virtanen, R., Riekkinen, P., 1992. Continuous α2-adrenoceptor blockade by atipamezole decreases neocortical high-voltage spindle activity in rats. Eur. J. Pharmacol. https://doi.org/10.1016/0014-2999(92)90722-G

Jankowsky, J.L., Fadale, D.J., Anderson, J., Xu, G.M., Gonzales, V., Jenkins, N.A., Copeland, N.G., Lee, M.K., Younkin, L.H., Wagner, S.L., Younkin, S.G., Borchelt, D.R., 2004. Mutant presenilins specifically elevate the levels of the 42 residue β-amyloid peptide in vivo: Evidence for augmentation of a 42-specific γ secretase. Hum. Mol. Genet. https://doi.org/10.1093/hmg/ddh019

Jo, S., Yarishkin, O., Hwang, Y.J., Chun, Y.E., Park, M., Woo, D.H., Bae, J.Y., Kim, T., Lee, J., Chun, H., Park, H.J., Lee, D.Y., Hong, J., Kim, H.Y., Oh, S.J., Park, S.J., Lee, H., Yoon, B.E., Kim, Y., Jeong, Y., Shim, I., Bae, Y.C., Cho, J., Kowall, N.W., Ryu, H., Hwang, E., Kim, D., Lee, C.J., 2014. GABA from reactive astrocytes impairs memory in mouse models of Alzheimer's disease. Nat. Med. https://doi.org/10.1038/nm.3639

Jyoti, A., Plano, A., Riedel, G., Platt, B., 2010. EEG, activity, and sleep architecture in a transgenic AβPPswe/PSEN1A246E Alzheimer's disease mouse. J. Alzheimers. Dis. 22, 873–887. https://doi.org/10.3233/JAD-2010-100879

Kärkkäinen, E., Yavich, L., Miettinen, P.O., Tanila, H., 2015. Opposing effects of APP/PS1 and TrkB.T1 genotypes on midbrain dopamine neurons and stimulated dopamine release in vivo. Brain Res. 1622, 452–465. https://doi.org/10.1016/j.brainres.2015.07.006

Kondabolu, K., Roberts, E.A., Bucklin, M., McCarthy, M.M., Kopell, N., Han, X., 2016. Striatal cholinergic interneurons generate beta and gamma oscillations in the corticostriatal circuit and produce motor deficits. Proc. Natl. Acad. Sci. 113, E3159–E3168. https://doi.org/10.1073/pnas.1605658113

Kramer, M.A., Tort, A.B.L., Kopell, N.J., 2008. Sharp edge artifacts and spurious coupling in EEG frequency comodulation measures. J. Neurosci. Methods 170, 352–357. https://doi.org/10.1016/j.jneumeth.2008.01.020

Kulik, Á., Nakadate, K., Nyíri, G., Notomi, T., Malitschek, B., Bettler, B., Shigemoto, R., 2002. Distinct localization of GABAB receptors relative to synaptic sites in the rat cerebellum and ventrobasal thalamus. Eur. J. Neurosci. 15, 291–307. https://doi.org/10.1046/j.0953-816x.2001.01855.x

Leinonen, H., Lipponen, A., Gurevicius, K., Tanila, H., 2016. Normal Amplitude of Electroretinography and Visual Evoked Potential Responses in AβPP/PS1 Mice. J. Alzheimer's Dis. 51, 21–26. https://doi.org/10.3233/JAD-150798

Letts, V.A., Beyer, B.J., Frankel, W.N., 2014. Hidden in plain sight: Spike-wave discharges in mouse inbred strains. Genes, Brain Behav. 13, 519–526. https://doi.org/10.1111/gbb.12142

Lüttjohann, A., Schoffelen, J.M., van Luijtelaar, G., 2013. Peri-ictal network dynamics of spike-wave discharges: Phase and spectral characteristics. Exp. Neurol. 239, 235–247. https://doi.org/10.1016/j.expneurol.2012.10.021

Maatuf, Y., Stern, E.A., Slovin, H., 2016. Abnormal Population Responses in the Somatosensory Cortex of Alzheimer's Disease Model Mice. Sci. Rep. 6. https://doi.org/10.1038/srep24560

Machová, E., Jakubík, J., Michal, P., Oksman, M., Iivonen, H., Tanila, H., Doležal, V., 2008. Impairment of muscarinic transmission in transgenic APPswe/PS1dE9 mice. Neurobiol. Aging 29, 368–378. https://doi.org/10.1016/j.neurobiolaging.2006.10.029

Machová, E., Rudajev, V., Smyčková, H., Koivisto, H., Tanila, H., Doležal, V., 2010. Functional cholinergic damage develops with amyloid accumulation in young adult APPswe/PS1dE9 transgenic mice. Neurobiol. Dis. 38, 27–35. https://doi.org/10.1016/j.nbd.2009.12.023

Meeren, H., Van Luijtelaar, G., Lopes Da Silva, F., Coenen, A., 2005. Evolving concepts on the pathophysiology of absence seizures: The cortical focus theory. Arch. Neurol. https://doi.org/10.1001/archneur.62.3.371

Midzianovskaia, I.S., Kuznetsova, G.D., Coenen, A.M.L., Spiridonov, A.M., Van Luijtelaar, E.L.J.M., 2001. Electrophysiological and pharmacological characteristics of two types of spike-wave discharges in WAG/Rij rats. Brain Res. 911, 62–70. https://doi.org/10.1016/S0006-8993(01)02705-6

Minkeviciene, R., Ihalainen, J., Malm, T., Matilainen, O., Keksa-Goldsteine, V., Goldsteins, G., Iivonen, H., Leguit, N., Glennon, J., Koistinaho, J., Banerjee, P., Tanila, H., 2008. Age-related decrease in stimulated glutamate release and vesicular glutamate transporters in APP/PS1 transgenic and wild-type mice. J. Neurochem. 105, 584–594. https://doi.org/10.1111/j.1471-4159.2007.05147.x

Minkeviciene, R., Rheims, S., Dobszay, M.B., Zilberter, M., Hartikainen, J., Fülöp, L., Penke, B., Zilberter, Y., Harkany, T., Pitkänen, A., Tanila, H., 2009. Amyloid beta-induced neuronal hyperexcitability triggers progressive epilepsy. J. Neurosci. 29, 3453–3462. https://doi.org/10.1523/JNEUROSCI.5215-08.2009

Mucke, L., Masliah, E., Yu, G.Q., Mallory, M., Rockenstein, E.M., Tatsuno, G., Hu, K., Kholodenko, D., Johnson-Wood, K., McConlogue, L., 2000. High-level neuronal expression of abeta 1-42 in wild-type human amyloid protein precursor transgenic mice: synaptotoxicity without plaque formation. J. Neurosci. 20, 4050–8. https://doi.org/20/11/4050 [pii]

Nygaard, H.B., Kaufman, A.C., Sekine-Konno, T., Huh, L.L., Going, H., Feldman, S.J., Kostylev, M.A., Strittmatter, S.M., 2015. Brivaracetam, but not ethosuximide, reverses memory impairments in an Alzheimer's disease mouse model. Alzheimers. Res. Ther. 7, 25. https://doi.org/10.1186/s13195-015-0110-9

Palop, J.J., Chin, J., Roberson, E.D., Wang, J., Thwin, M.T., Bien-Ly, N., Yoo, J., Ho, K.O., Yu, G.Q., Kreitzer, A., Finkbeiner, S., Noebels, J.L., Mucke, L., 2007. Aberrant Excitatory Neuronal Activity and Compensatory Remodeling of Inhibitory Hippocampal Circuits in Mouse Models of Alzheimer's Disease. Neuron 55, 697–711. https://doi.org/10.1016/j.neuron.2007.07.025

Papazoglou, A., Soos, J., Lundt, A., Wormuth, C., Ginde, V.R., Müller, R., Henseler, C., Broich, K., Xie, K., Ehninger, D., Haenisch, B., Weiergräber, M., 2016. Gender-Specific Hippocampal Dysrhythmia and Aberrant Hippocampal and Cortical Excitability in the APPswePS1dE9 Model of Alzheimer's Disease. Neural Plast. 2016. https://doi.org/10.1155/2016/7167358

Papazoglou, A., Soos, J., Lundt, A., Wormuth, C., Ginde, V.R., Müller, R., Henseler, C., Broich, K., Xie, K., Haenisch, B., Ehninger, D., Weiergräber, M., 2017. Motor cortex theta and gamma architecture in young adult APPswePS1dE9 Alzheimer mice. PLoS One 12. https://doi.org/10.1371/journal.pone.0169654

Paxinos, G., Franklin, K.B.J., 2004. The mouse brain in stereotaxic coordinates, Academic Press. https://doi.org/10.1016/S0306-4530(03)00088-X

Perez, S.E., Lazarov, O., Koprich, J.B., Chen, E.-Y., Rodriguez-Menendez, V., Lipton, J.W., Sisodia, S.S., Mufson, E.J., 2005. Nigrostriatal Dysfunction in Familial Alzheimer's Disease-Linked APPswe/PS1ΔE9 Transgenic Mice. J. Neurosci. 25, 10220–10229. https://doi.org/10.1523/JNEUROSCI.2773-05.2005

Pinault, D., Vergnes, M., Marescaux, C., 2001. Medium-voltage 5-9-Hz oscillations give rise to spike-and-wave discharges in a genetic model of absence epilepsy: In vivo dual extracellular recording of thalamic relay and reticular neurons. Neuroscience. https://doi.org/10.1016/S0306-4522(01)00182-8

Riekkinen, P., Aaltonen, M., Riekkinen, P., 1991. Tetrahydroaminoacridine inhibits high voltage spindle activity in aged rats after acute and chronic treatment. Psychopharmacology (Berl). 103, 265–267. https://doi.org/10.1007/BF02244214

Riekkinen, P., Riekkinen, M., Sirviö, J., Riekkinen, P., 1992. Neurophysiological consequences of combined cholinergic and noradrenergic lesions. Exp. Neurol. https://doi.org/10.1016/0014-4886(92)90176-Q

Riekkinen, P., Sirviö, J., Riekkinen, P., 1990. Relationship between the cortical choline acetyltransferase content and EEG delta-power. Neurosci. Res. 8, 12–20. https://doi.org/10.1016/0168-0102(90)90052-G

Roberson, E.D., Scearce-Levie, K., Palop, J.J., Yan, F., Cheng, I.H., Wu, T., Gerstein, H., Yu, G.-Q., Mucke, L., 2007. Reducing endogenous tau ameliorates amyloid beta-induced deficits in an Alzheimer's disease mouse model. Science 316, 750–4. https://doi.org/10.1126/science.1141736

Russo, E., Citraro, R., Constanti, A., Leo, A., Lüttjohann, A., van Luijtelaar, G., De Sarro, G., 2016. Upholding WAG/Rij rats as a model of absence epileptogenesis: Hidden mechanisms and a new theory on seizure development. Neurosci. Biobehav. Rev. https://doi.org/10.1016/j.neubiorev.2016.09.017

Sanchez, P.E., Zhu, L., Verret, L., Vossel, K.A., Orr, A.G., Cirrito, J.R., Devidze, N., Ho, K., Yu, G.-Q., Palop, J.J., Mucke, L., 2012. Levetiracetam suppresses neuronal network dysfunction and reverses synaptic and cognitive deficits in an Alzheimer's disease model. Proc. Natl. Acad. Sci. 109, E2895–E2903. https://doi.org/10.1073/pnas.1121081109

Scarmeas, N., Honig, L.S., Choi, H., Cantero, J., Brandt, J., Blacker, D., Albert, M., Amatniek, J.C., Marder, K., Bell, K., Hauser, W.A., Stern, Y., 2009. Seizures in Alzheimer disease: who, when, and how common? Arch. Neurol. 66, 992–7. https://doi.org/10.1001/archneurol.2009.130

Sharott, A., Magill, P.J., Harnack, D., Kupsch, A., Meissner, W., Brown, P., 2005. Dopamine depletion increases the power and coherence of β-oscillations in the cerebral cortex and subthalamic nucleus of the awake rat. Eur. J. Neurosci. 21, 1413–1422. https://doi.org/10.1111/j.1460-9568.2005.03973.x

Sorokin, J.M., Paz, J.T., Huguenard, J.R., 2016. Absence seizure susceptibility correlates with pre-ictal β oscillations. J. Physiol. Paris. https://doi.org/10.1016/j.jphysparis.2017.05.004

Swerdlow, N.R., Geyer, M.A., Braff, D.L., 2001. Neural circuit regulation of prepulse inhibition of startle in the rat: Current knowledge and future challenges. Psychopharmacology (Berl). https://doi.org/10.1007/s002130100799

Timofeev, I., Steriade, M., 2004. Neocortical seizures: Initiation, development and cessation. Neuroscience. https://doi.org/10.1016/j.neuroscience.2003.08.051

Tort, A.B.L., Komorowski, R.W., Manns, J.R., Kopell, N.J., Eichenbaum, H., 2009. Theta-gamma coupling increases during the learning of item-context associations. Proc. Natl. Acad. Sci. 106, 20942–20947. https://doi.org/10.1073/pnas.0911331106

Tort, A.B.L., Kramer, M.A., Thorn, C., Gibson, D.J., Kubota, Y., Graybiel, A.M., Kopell, N.J., 2008. Dynamic cross-frequency couplings of local field potential oscillations in rat striatum and hippocampus during performance of a T-maze task. Proc. Natl. Acad. Sci. 105, 20517–20522. https://doi.org/10.1073/pnas.0810524105

Ulrich, D., 2015. Amyloid- Impairs Synaptic Inhibition via GABAA Receptor Endocytosis. J. Neurosci. 35, 9205–9210. https://doi.org/10.1523/JNEUROSCI.0950-15.2015

Van Lier, H., Drinkenburg, W.H.I.M., Van Eeten, Y.J.W., Coenen, A.M.L., 2004. Effects of diazepam and zolpidem on EEG beta frequencies are behavior-specific in rats. Neuropharmacology 47, 163–174. https://doi.org/10.1016/j.neuropharm.2004.03.017

Vergnes, M., Marescaux, C., Depaulis, A., Micheletti, G., Warter, J.M., 1987. Spontaneous spike and wave discharges in thalamus and cortex in a rat model of genetic petit mal-like seizures. Exp. Neurol. 96, 127–136. https://doi.org/10.1016/0014-4886(87)90174-9

Vossel, K.A., Ranasinghe, K.G., Beagle, A.J., Mizuiri, D., Honma, S.M., Dowling, A.F., Darwish, S.M., Van Berlo, V., Barnes, D.E., Mantle, M., Karydas, A.M., Coppola, G., Roberson, E.D., Miller, B.L., Garcia, P.A., Kirsch, H.E., Mucke, L., Nagarajan, S.S., 2016. Incidence and impact of subclinical epileptiform activity in Alzheimer's disease. Ann. Neurol. 80, 858–870. https://doi.org/10.1002/ana.24794

Vossel, K.A., Tartaglia, M.C., Nygaard, H.B., Zeman, A.Z., Miller, B.L., 2017. Epileptic activity in Alzheimer's disease: causes and clinical relevance. Lancet Neurol. https://doi.org/10.1016/S1474-4422(17)30044-3

Wang, J., Ikonen, S., Gurevicius, K., Van Groen, T., Tanila, H., 2002. Alteration of cortical EEG in mice carrying mutated human APP transgene. Brain Res. 943, 181–190. https://doi.org/10.1016/S0006-8993(02)02617-3

Westmark, C.J., Westmark, P.R., Beard, A.M., Hildebrandt, S.M., Malter, J.S., 2008. Seizure susceptibility and mortality in mice that over-express amyloid precursor protein. Int. J. Clin. Exp. Pathol. 1, 157–68.

Westmark, C.J., Westmark, P.R., Malter, J.S., 2010. Alzheimer's Disease and Down Syndrome Rodent Models Exhibit Audiogenic Seizures. J. Alzheimers. Dis. 20, 1009–1013. https://doi.org/10.3233/JAD-2010-100087

Zilberter, M., Ivanov, A., Ziyatdinova, S., Mukhtarov, M., Malkov, A., Alpár, A., Tortoriello, G., Botting, C.H., Fülöp, L., Osypov, A.A., Pitkänen, A., Tanila, H., Harkany, T., Zilberter, Y., 2013. Dietary energy substrates reverse early neuronal hyperactivity in a mouse model of Alzheimer's disease. J. Neurochem. 125, 157–171. https://doi.org/10.1111/jnc.12127

Ziyatdinova, S., Rönnbäck, A., Gurevicius, K., Miszczuk, D., Graff, C., Winblad, B., Pitkänen, A., Tanila, H., 2016. Increased Epileptiform EEG Activity and Decreased Seizure Threshold in Arctic APP Transgenic Mouse Model of Alzheimer's Disease. Curr. Alzheimer Res. 13, 817–30. https://doi.org/10.2174/1567205013666160129095508

Figure legends

Figure 1. Schematic drawings (modified from Paxinos & Franklin, 2004 (Paxinos and Franklin, 2004)) showing LFP recording sites in superficial (sFC) and medial (mFC) frontal cortex, parietal cortex (PC), hippocampus (HC), thalamus (TH), superficial (sVC) and deep (dVC) visual cortex. The sFC and PC depict skull screw electrodes, which in reality were located on the opposite side from the corresponding wire electrodes. The histological sections of the corresponding brain locations are projected to the opposite hemisphere for illustration purposed. Amyloid plaques show up as dark spots throughout all cortical layers, more layer specifically in the hippocampus and only as scattered spots in the thalamus (anti-human Aβ staining). Scale bars: 500 µm.

Figure 2. Mean power spectral density of middle-aged APP/PS1 (TG, red lines, n = 14) and wild-type (WT, black lines, n = 16) mice from 3 to 140 Hz in different brain regions under different behavioral states. Artifacts at 48-52 and 99-101 Hz were removed by interpolating two neighboring points. For better visualization the spectrum was whitened by multiplying with the square of frequency $(f)^2$. Light green shading indicates 1 Hz frequency bins where APP/PS1 mice significantly ($p < 0.05$) differ from WT littermates (two-sample t-test with false discovery rate correction). mFC = wire electrode in medial frontal cortex, sFC = screw electrode above the frontal cortex, PC = screw electrode above the parietal cortex, DG = wire electrode in the dentate gyrus, TH = wire electrode in the lateral geniculate nucleus of the thalamus, sVC and dVC = wire electrode in superficial vs. deep layers of visual cortex.

Figure 3. Mean (± SEM) power spectral density of 4-month-old wild-type (WT, Y, n =7) and APP/PS1 mice (TG, Y, n = 10), and 14- to 16-month-old wild-type (WT, O, n = 16) and APP/PS1 (TG, O, n = 14) mice in conventional frequency bands: delta (1-4 Hz), theta (5-9 Hz), alpha (10-15 Hz), beta (16 – 29 Hz), and gamma (30 – 100 Hz). The y-axis values represent power without whitening. However, to remove possible error due to different amplification, the values have been normalized so that the group means of young and middle-aged WT mice are equal. **significant genotype effect, $p < 0.01$; ***significant genotype effect, $p < 0.001$; $^{\#\#}$ significant age x genotype interaction, $p < 0.01$; two-way ANOVA.

Figure 4. Spatial distribution of SWD events in APP/PS1 mice. (**A**) A typical SWD recorded in the frontal surface channel on the left hemisphere (sFC (L)) is highlighted with red color. The event appears similar in the right parietal surface channel (sPC (R)) but is not detected in the superficial

layers of visual cortex on the left (sVC (L)), right medial frontal cortex (mFC (R)) or right dentate gyrus (DG (R)). (**B**) Another SWD over the left frontal cortex. The thalamic channel (Po nucleus) on the same hemisphere shows synchronized spiking of opposite polarity, whereas the right DG does not. (**C, D**) corresponding spectral distribution of power during the SWD events marked in red color.

Figure 5. (A) Example of the custom-made user interface to augment detection of SWD events. Recording from the frontal screw electrode (sFC channel). Top: raw EEG data (blue line); bottom: data filtered between 7-23 Hz (black line), its envelope (red line) and threshold (dashed grey line, at mean+2.7 SD in this mouse). Green and red filled triangles indicate the start and end of the SWD event. Note the high-frequency EMG artefact on the raw EEG (red triangle) associated with a small head movement right after the SWD. (**B**) Mean (+SEM) number of SWDs and their mean duration in WT (gray-black) and APP/PS1 (pink-red) young (Y) and middle-aged (O) mice. *** significant genotype effect, $p < 0.001$; ### significant age effect, $p < 0.001$; two-way ANOVA. (**C**) Comparison of mean PSDs between raw (solid lines) and SWD-depleted EEG (dashed lines) in middle-aged mice of both genotypes. Removal of SWDs did not significantly impact the PSDs.

Figure 6. Temporal distribution of pre-SWD 20-40 Hz, 6-12 Hz and 2-4 + 6-12 Hz power in APP/PS1 mice. The 60-s epoch before the onset of each SWD event was divided into 30 bins (2 s / bin), and then power of frequency bands was calculated for each bin. Paired-samples t-test was applied to compare PSD means between each pair of neighboring bins, and the 0-30s vs. 31-60s preceding the SWDs. Power at 20-40 Hz during the second half of 60-s epoch preceding the SWD was significantly higher than the first half both in WT (n=56) and APP/PS1 (n=240) groups, while 6-12Hz power increased only in APP/PS1 mice (*$p < 0.05$, paired-samples t-test). In addition, the power in the 2-s bin immediately preceding the SWD was significantly higher than during the preceding bin in 6-12 Hz and combined 2-4 + 6-12 Hz power bands (*$p < 0.05$, paired-samples t-test).

Figure 7. Co-modulation between delta phase and high-gamma amplitude. (**A**) An example of bicoherence plot reflecting interacting frequency bands in mFC of a WT mouse during NREM sleep. The arrowhead points to 2.8 Hz that has the highest co-modulation with the high-gamma band (70-100 Hz). (**B**) Top: an excerpt of EEG recorded from the mFC electrode in the same mouse. Note the prominent gamma oscillations riding on the delta peaks; Bottom: filtered EEG to show the synchronized delta (1-4 Hz) and gamma (70-100 Hz) oscillations. (**C**) Comparison

between observed MI from original data and surrogate MI from shuffled data. During waking immobility (WI) and NREM sleep mFC showed significantly higher observed MI than surrogate MI (threshold set at p = 0.01) in both WT and TG mice. Besides, significant co-modulation was discovered in DG during NREM sleep. (**D**) MI comparison between WT and TG mice in mFC and DG. In mFC, MI differed between behavioral states but not between genotypes; in DG, the difference in MI was both behavior- and genotype-dependent. For all cases, Friedman's test was applied, (*)p=0.052, *p<0.05, **p<0.01, ***p<0.001; error bars show mean±SEM. Red asterisks refer to state differences in TG mice, black to state differences in WT mice, and blue ones genotype differences. Ns: WT 16, TG 14.

Figure 8. Co-modulation between theta phase and gamma amplitude. (**A**) An example of bicoherence plot showing interacting frequency bands in DG of a TG mouse during movement (Mov). The arrowhead points to 7.7 Hz that has highest interaction with gamma band (60 – 100 Hz). (**B**) Top: EEG excerpt from DG of the same mouse. Note the gamma oscillations riding on theta troughs. Bottom: filtered EEG to show the synchronized theta (6-10 Hz) and gamma (60-100 Hz) oscillations. (**C**) Comparison between observed MI from original data and surrogate MI from shuffled data. MIs in mFC, DG, TH and dVC were higher than the chance level (surrogate MI threshold at p = 0.01). (**D**) MI comparison between the genotypes and behavioral states in mFC, DG, TH and dVC. In DG and dVC, the MI was only behavior-dependent; in mFC and TH, neither genotype nor behavioral states differentiated MI levels. For all cases, Friedman's test was applied, *p<0.05, **p<0.01, ***p<0.001; error bars show mean±SEM. Red asterisks refer to state differences in TG mice, black to state differences in WT mice. Ns: WT 16, TG 14.

Figure 9. Auditory evoked potentials (AEPs) in young and middle-aged APP/PS1 vs. WT mice in the auditory gating paradigm. (**A**) Averaged cortical AEPs in WT and APP/PS1 (TG) mice responding to conditioning stimulus (cond.) and test stimulus (test), showing a consistent surface-negative trough (N1) followed by a surface-positive peak (P2). The red shadow shows SEM for the response to the conditioning stimulus and the black shadow for the test stimulus. The tone onset was at 100 ms (filled triangle) from the start of each sweep. (**B1**) Averaged peak N1 and P2 amplitudes and (**B2**) latencies for young (Y) and middle-aged (O) WT and APP/PS1 mice. Significance levels: ** significant genotype difference, $p < 0.01$; $^{###}$ significant age difference (may be due to different ampligication), $p < 0.001$; two-way ANOVA. (**C**) Auditory gating (habituation of the P2-N1 difference between responses to conditioned and test tones) in young (Y) and middle-

aged (O) WT and APP/PS1 mice. No genotype or age effect or their interaction was found. Ns: WT(Y) 7, TG (Y) 10, WT(O) 16, TG (O) 14.

Figure 10. Acoustic and spontaneous startle reactivity of APP/PS1 and wild-type mice from 3 to 11 months of age. (A) Acoustic startle and pre-pulse inhibition with 0, 20, 35and 50 dB pre-pulse at 3 months, (B) 8 months, (C) 11 months. (D) Spontaneous startles as a proxy of myoclonus at 3-11 months of age. The y-axis denote observed startles that exceed the virtual body weight threshold of 10 g. (E) Development of mean body weight across ages. Error bars: mean±SEM. *p<0.05; **p<0.01 in ANOVA for repeated measures. WT: wild type, TG: transgenic. Ns: WT 8, TG 9.

Figure 1

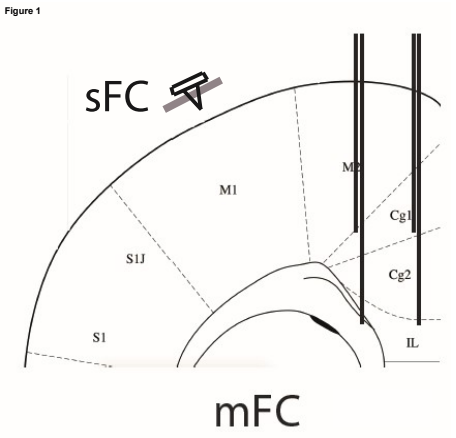

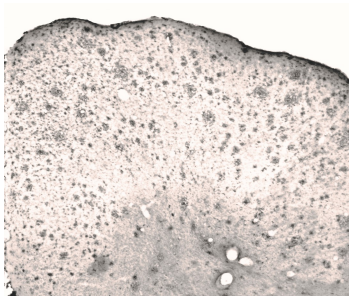

mFC

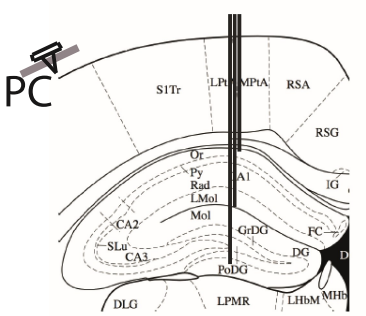

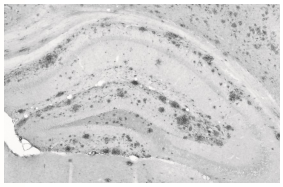

HC

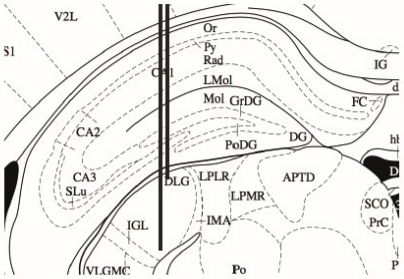

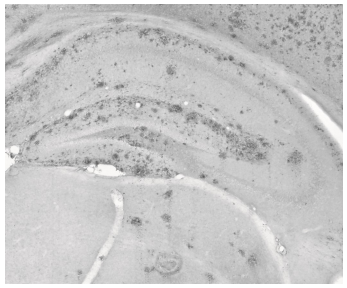

TH

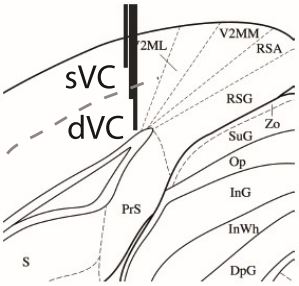

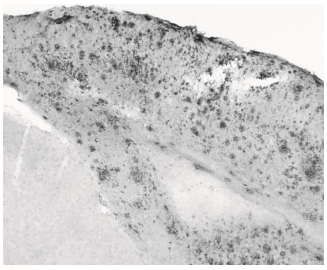

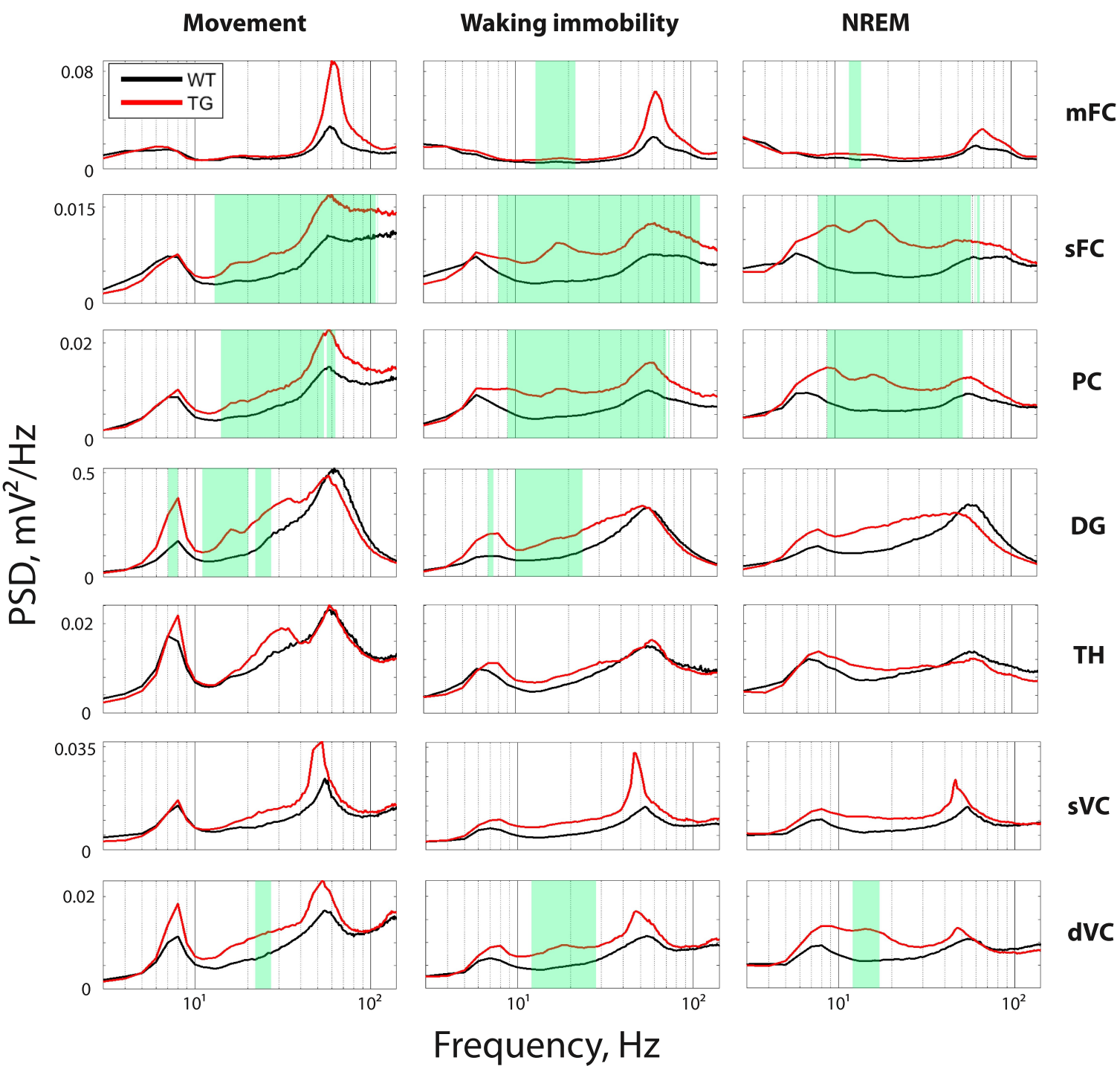
Movement
Waking immobility
NREM
WT
TG
mFC
sFC
PC
DG
TH
sVC
dVC
0.08
0
0.015
0
0.02
0
0.5
0
0.02
0
0.035
0
0.02
0
10^1
10^2
PSD, mV²/Hz
Frequency, Hz

Figure 3

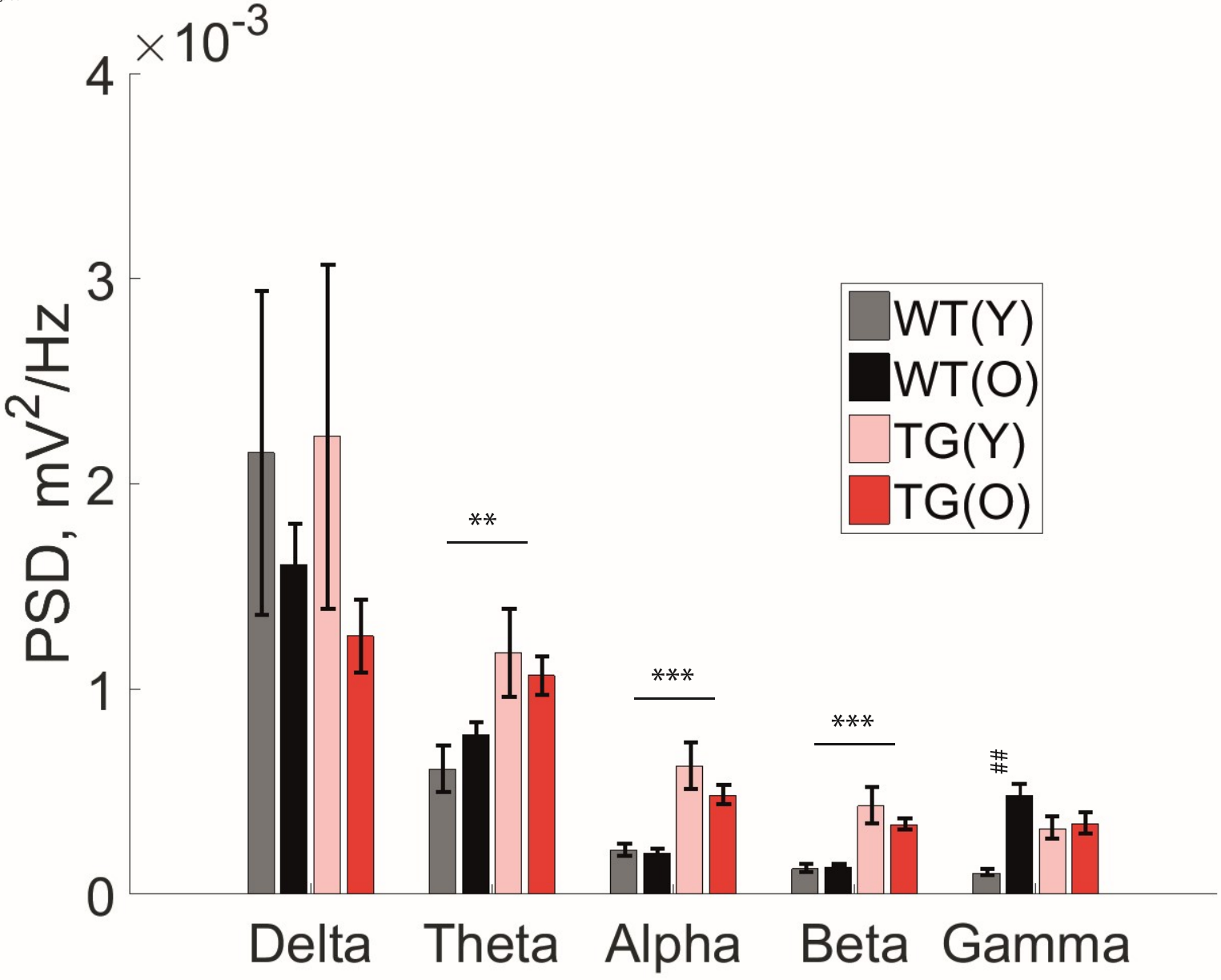
×10-3
4
3
2
1
0
PSD, mV2/Hz
WT(Y)
WT(O)
TG(Y)
TG(O)
**
***
***
##
Delta
Theta
Alpha
Beta
Gamma

Figure 4

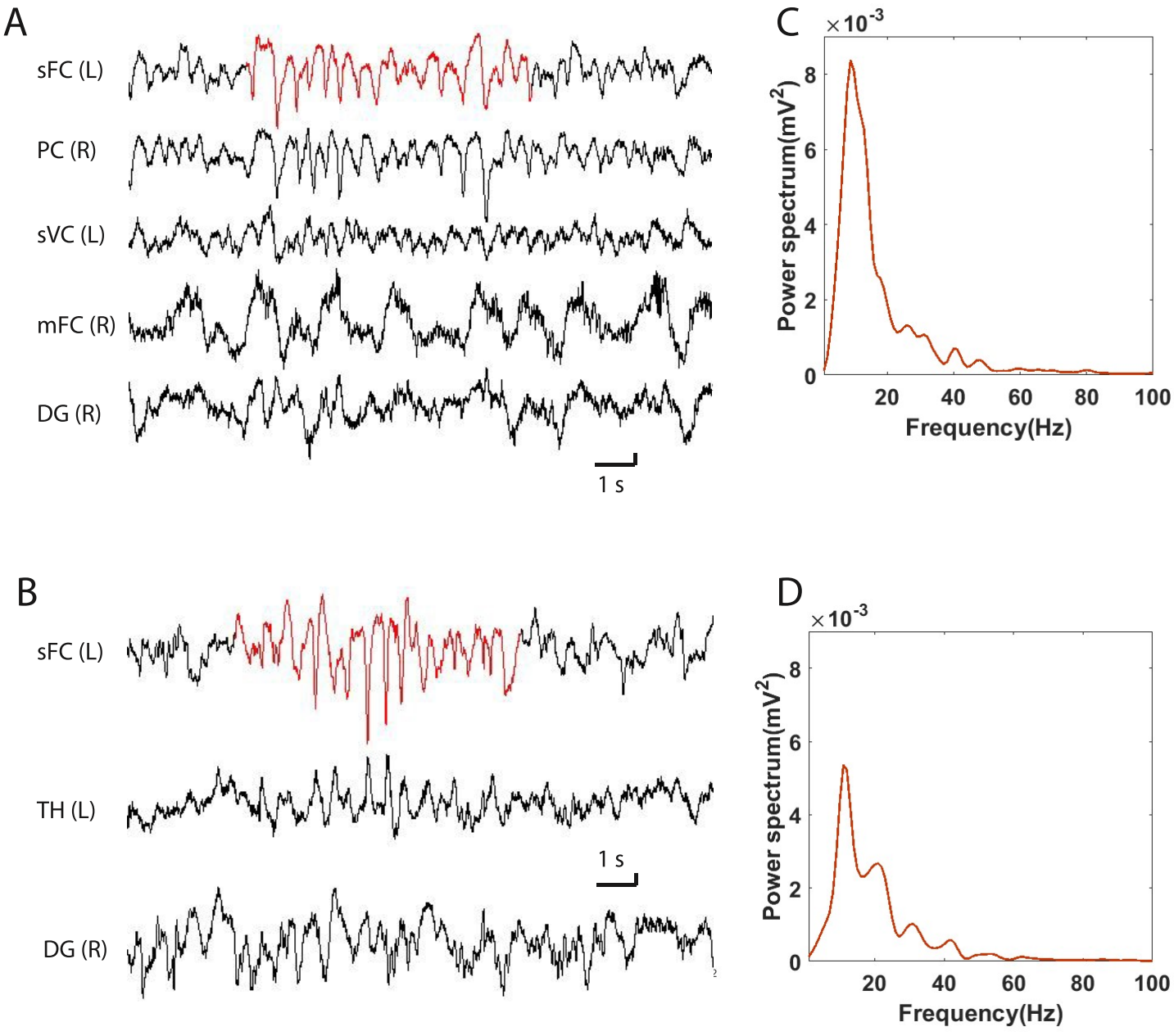
A
sFC (L)
PC (R)
sVC (L)
mFC (R)
DG (R)
1 s
C
×10^-3
Power spectrum(mV^2)
Frequency(Hz)
B
sFC (L)
TH (L)
1 s
DG (R)
D
×10^-3
Power spectrum(mV^2)
Frequency(Hz)

Figure 5

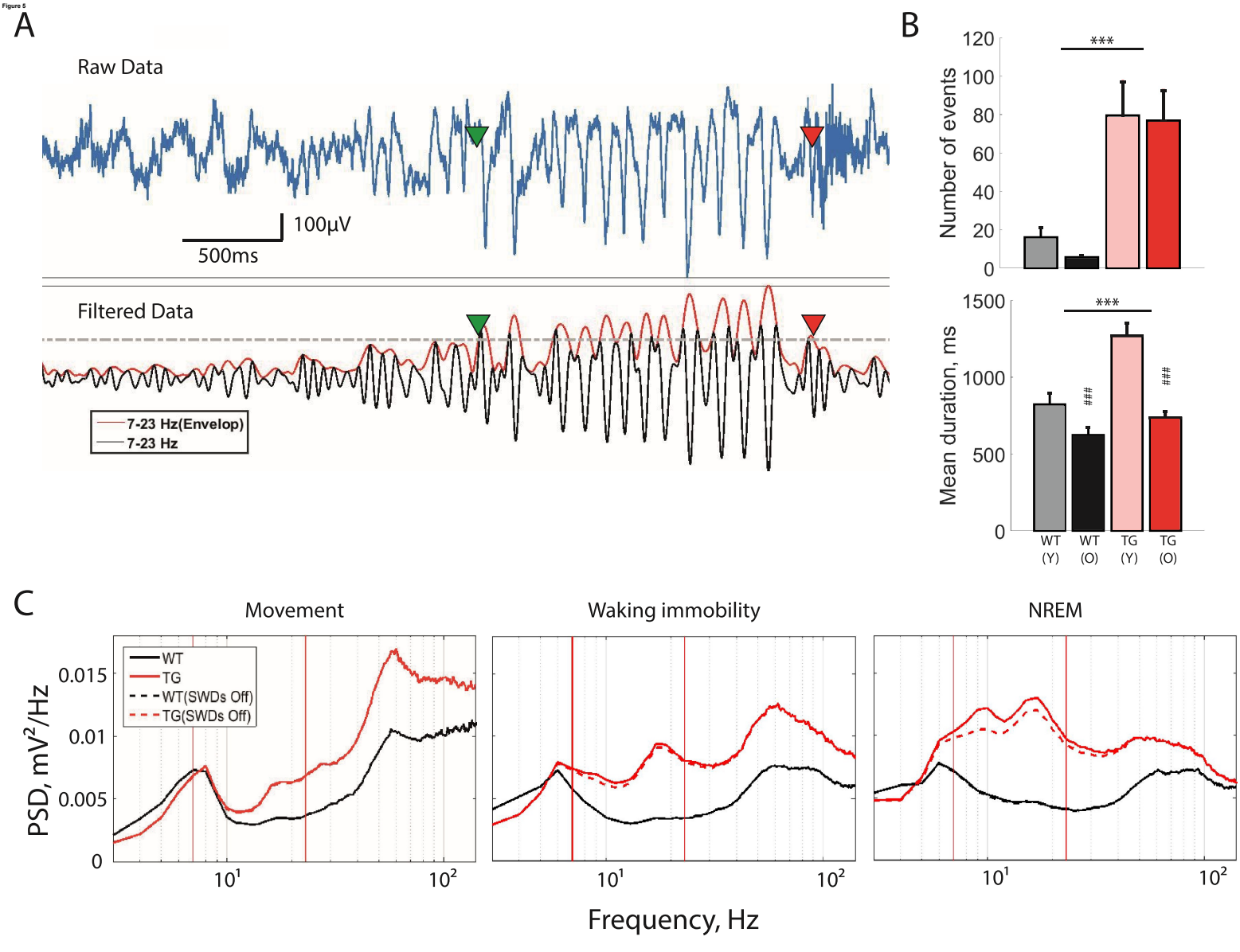
A
Raw Data
100µV
500ms
Filtered Data
7-23 Hz(Envelop)
7-23 Hz
B
Number of events
***
Mean duration, ms
***
###
###
WT (Y)
WT (O)
TG (Y)
TG (O)
C
Movement
Waking immobility
NREM
WT
TG
WT(SWDs Off)
TG(SWDs Off)
PSD, mV²/Hz
Frequency, Hz

Figure 6

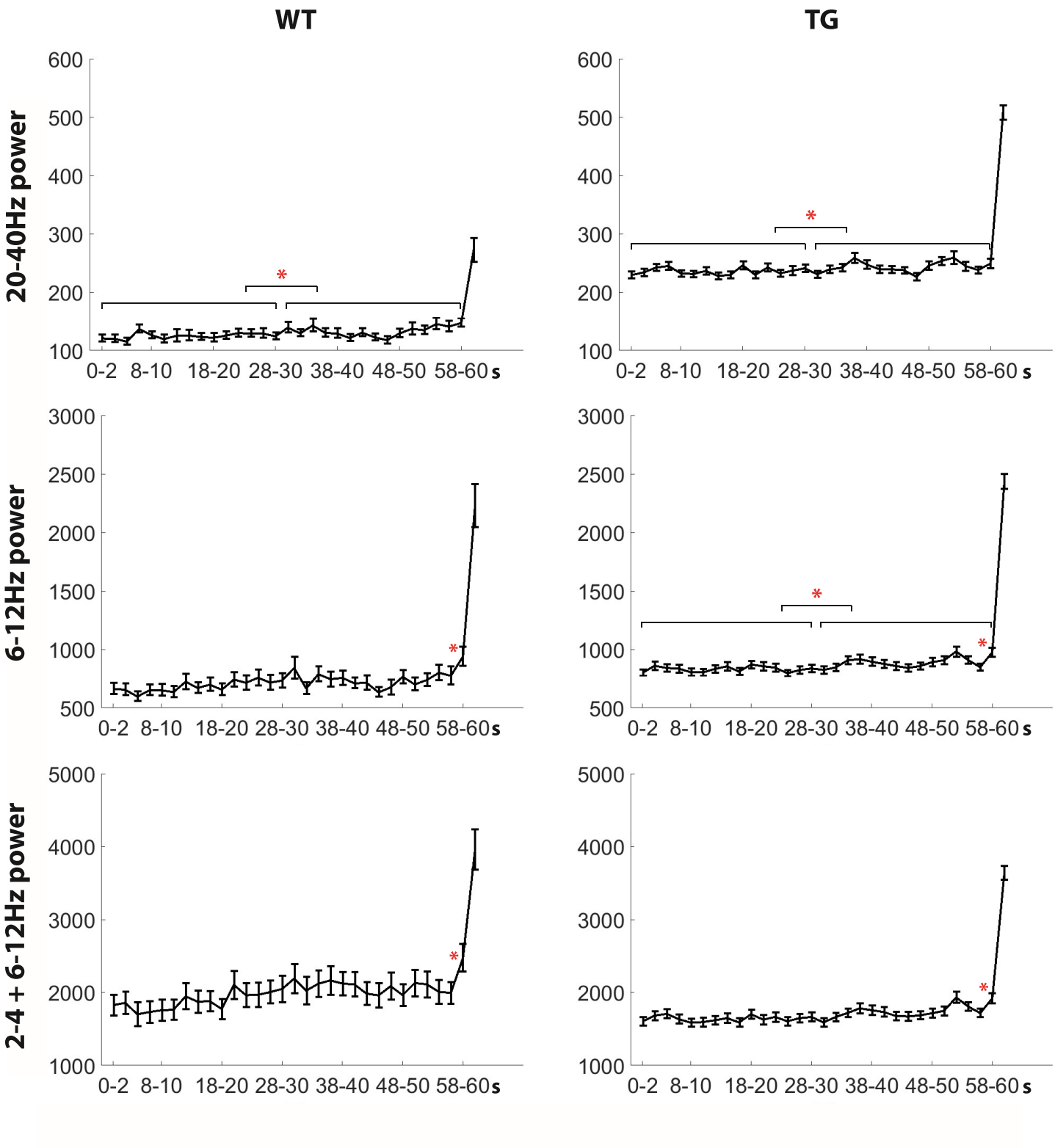
WT
TG
20-40Hz power
6-12Hz power
2-4 + 6-12Hz power
0-2 8-10 18-20 28-30 38-40 48-50 58-60 s

Figure 7

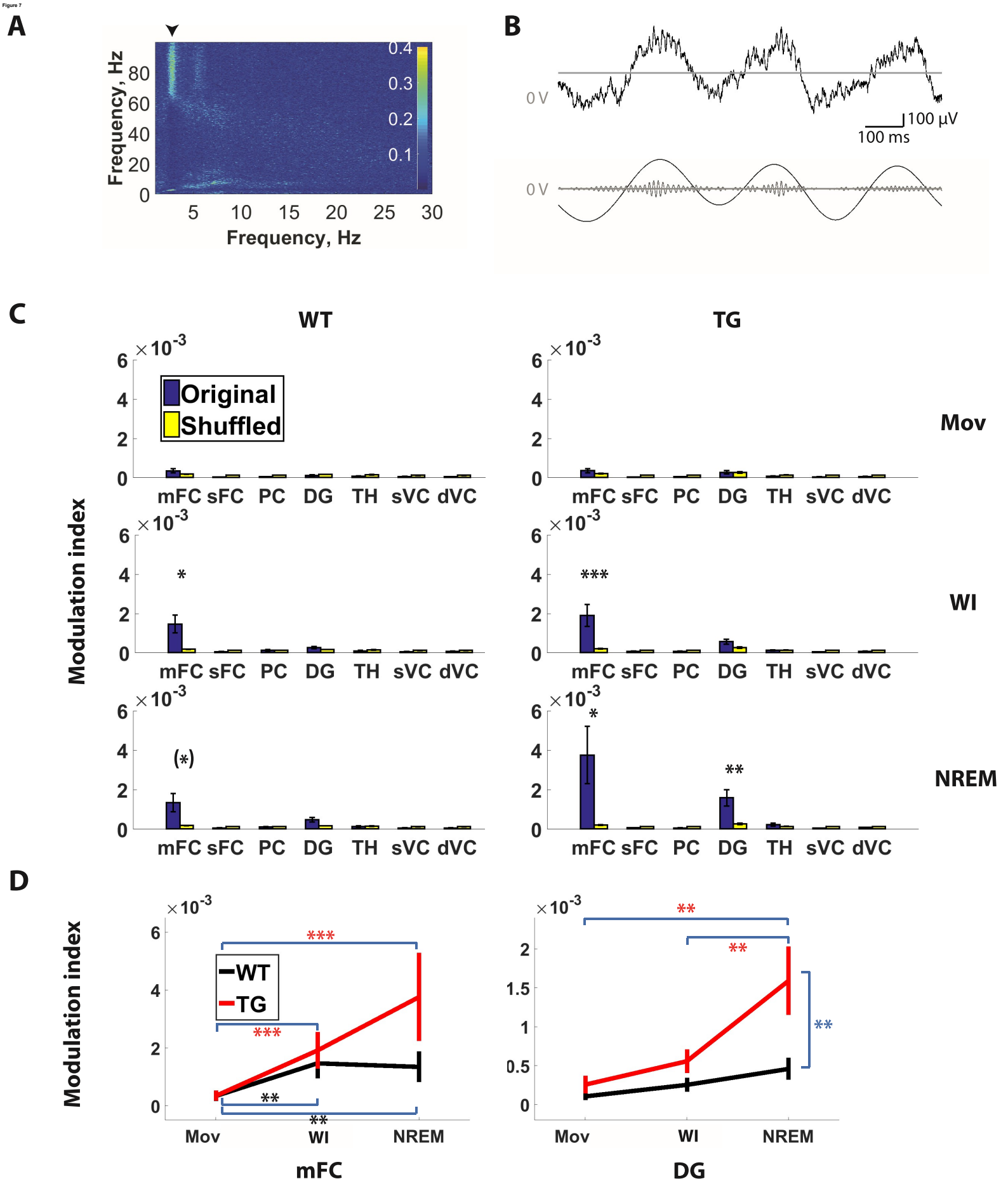
A
Frequency, Hz
Frequency, Hz
B
0 V
100 µV
100 ms
0 V
C
WT
TG
Original
Shuffled
Modulation index
Mov
WI
NREM
mFC sFC PC DG TH sVC dVC
D
WT
TG
Modulation index
Mov
WI
NREM
mFC
DG

Figure 8

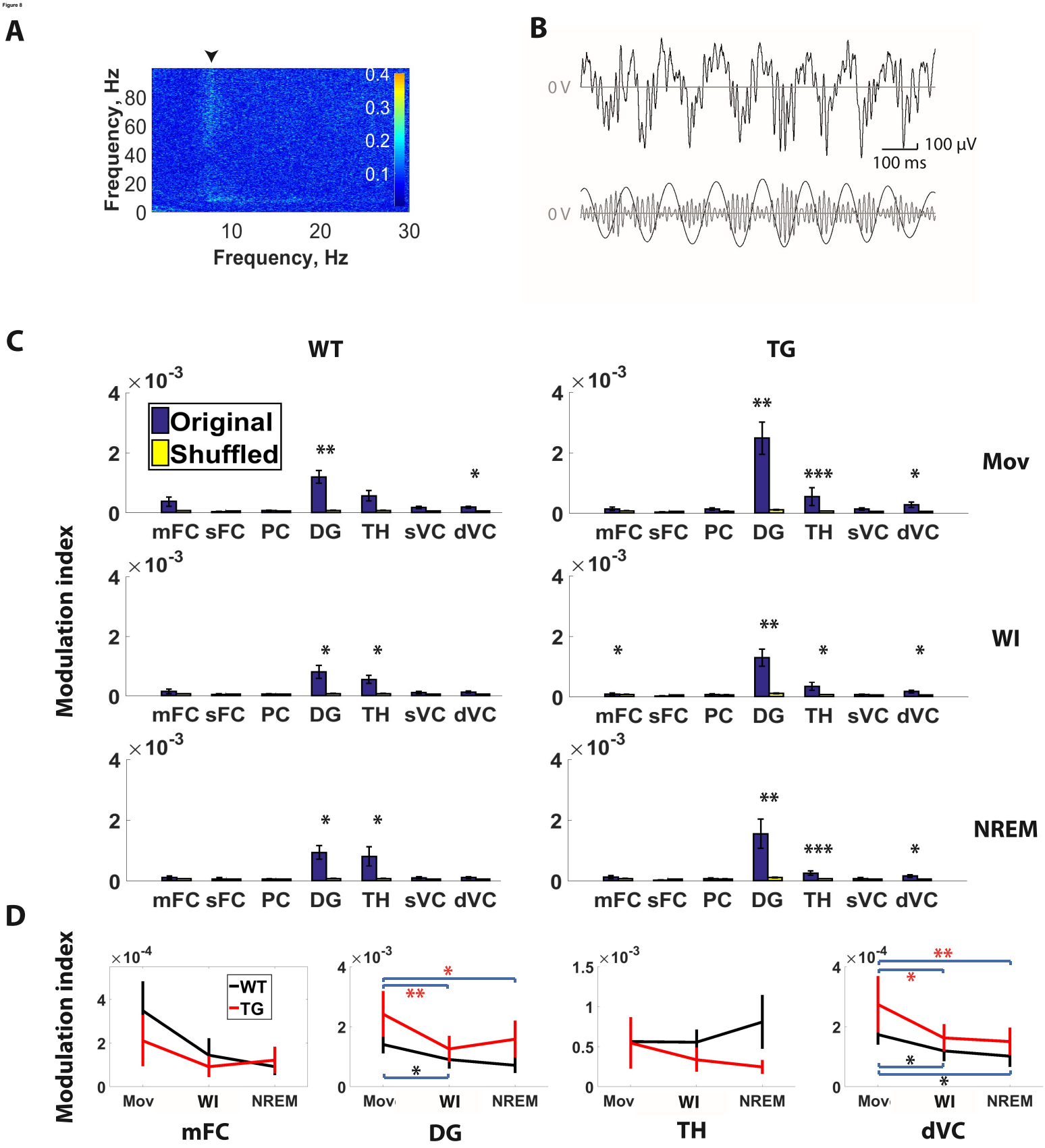
A
Frequency, Hz
80
60
40
20
0
10
20
30
Frequency, Hz
0.4
0.3
0.2
0.1
B
0 V
100 µV
100 ms
0 V
C
WT
TG
Original
Shuffled
Modulation index
×10-3
4
2
0
**
*
***
mFC sFC PC DG TH sVC dVC
Mov
WI
NREM
D
Modulation index
×10-4
×10-3
×10-3
×10-4
WT
TG
Mov
WI
NREM
mFC
DG
TH
dVC

Figure 9

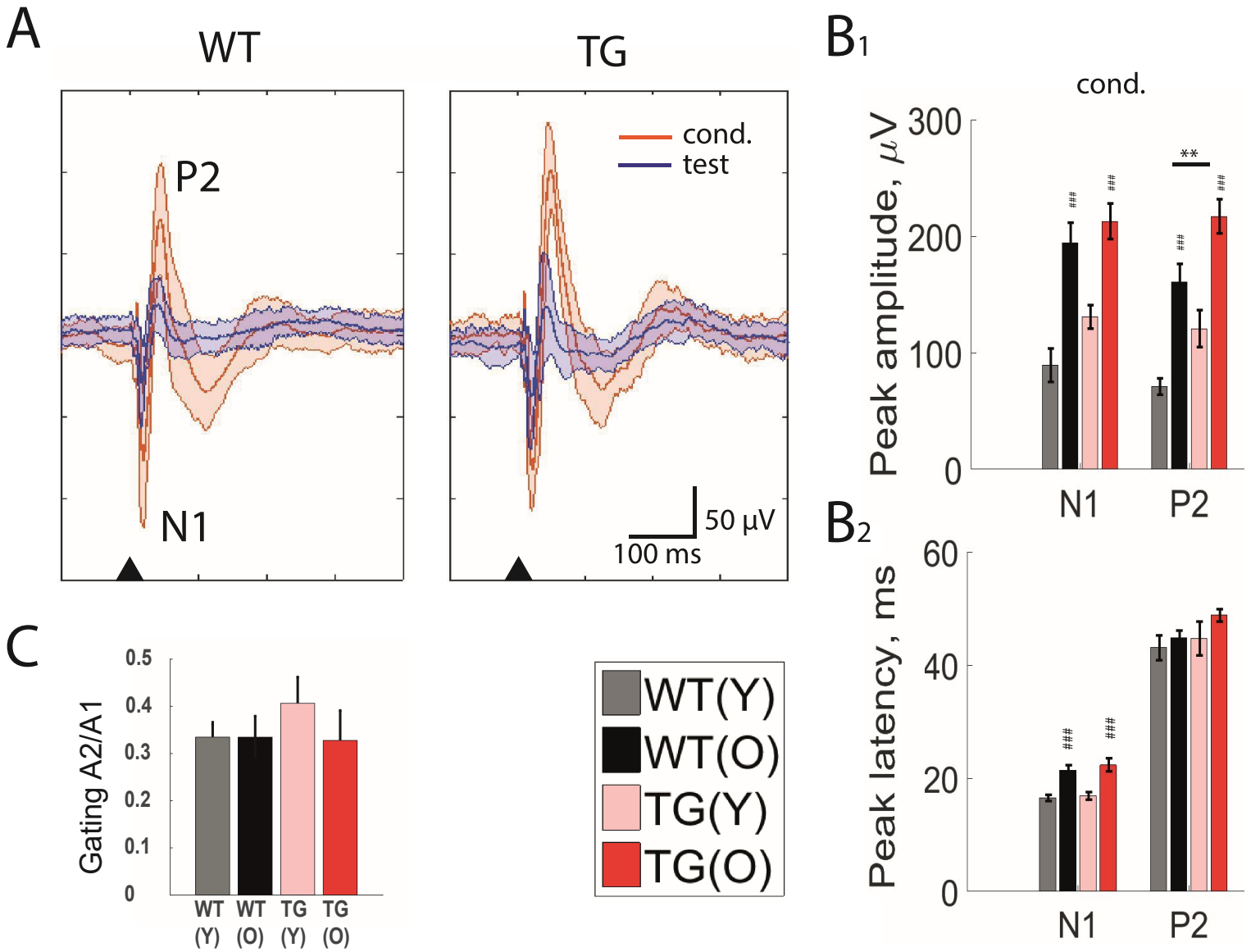
A
WT
TG
P2
N1
cond.
test
50 µV
100 ms
B1
cond.
Peak amplitude, µV
300
200
100
0
**
###
N1
P2
B2
Peak latency, ms
60
40
20
0
C
Gating A2/A1
0.5
0.4
0.3
0.2
0.1
0
WT (Y)
WT (O)
TG (Y)
TG (O)
WT(Y)
WT(O)
TG(Y)
TG(O)

Figure 10

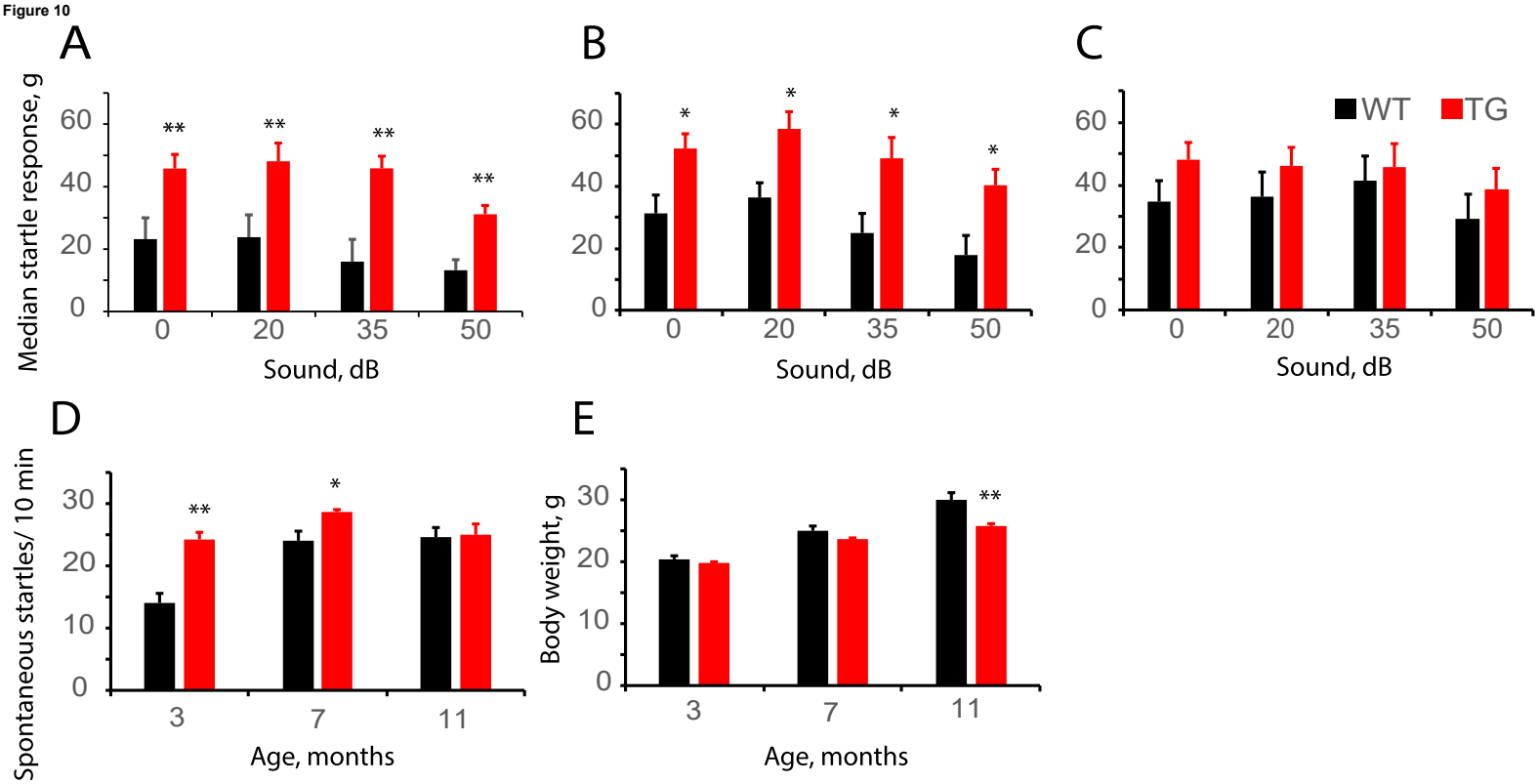
A
B
C
D
E
Median startle response, g
Sound, dB
WT
TG
Spontaneous startles/ 10 min
Age, months
Body weight, g
0
20
35
50
3
7
11
10
30
40
60
**
*

Table 1

Table 1. Number of recordings taken into analysis from different recording sites and genotypes. For each mouse, only the earliest qualified recording was analyzed; if all recordings from the same mouse were of bad quality, this mouse was excluded from the analysis. mFC: medial frontal cortex; sFC: superficial frontal cortex; PC: parietal cortex; DG: dentate gyrus; TH: thalamus; sVC: superficial visual cortex; dVC: deep visual cortex.

	mFC	**sFC**	**PC**	**DG**	**TH**	**sVC**	**dVC**
WT	13	16	16	9	9	9	13
TG	13	14	14	9	11	7	12